IEEE Access
Multidisciplinary | Rapid Review | Open Access Journal

Received September 6, 2021, accepted September 15, 2021, date of publication September 22, 2021,
date of current version October 6, 2021.

Digital Object Identifier 10.1109/ACCESS.2021.3114771

Deterministic 5G mmWave Large-Scale 3D Path Loss Model for Lagos Island, Nigeria

SIMON K. HINGA, (Graduate Student Member, IEEE), AND ADEREMI A. ATAYERO, (Member, IEEE)

Department of Electrical and Information Engineering, Covenant University, Ota 112212, Nigeria
IoT-Enabled Smart and Connected Communities (SmartCU) Research Cluster, Covenant University, Ota 112233, Nigeria

Corresponding author: Aderemi A. Atayero (atayero@cu.edu.ng)

This work was supported in part by the IoT-Enabled Smart and Connected Communities (SmartCU) Research Cluster, Covenant University, in part by the Covenant University Centre for Research, Innovation, and Development (CUCRID), in part by REMCOM Corporation, State College, PA, USA, and in part by Queen Elizabeth Commonwealth Scholarship Program.

ABSTRACT 5G millimeter wave (mmWave) application in mobile connectivity to realize high-speed, reliable communication is attributed with high path loss. This paper presents a detailed 3D ray-tracing technique at 28 GHz for Lagos Island to investigate five unique path loss scenarios: path loss, free space path loss with antenna pattern, free space path loss without antenna pattern, excess path loss with antenna pattern, and the excess path loss without antenna pattern for an urban environment. The Close-In (CI) model, Floating Intercept (FI) path loss model, and a root mean square error (RMSE) are used to model and evaluate the best path loss model for Lagos Island. The average achieved FI (α, β, σ) parameters were 189.92352, 0.1654, and 0.66948, While the average CI (η, $X\sigma$) parameters were 2.309355 and 56.236425. From all the scenarios evaluated, the lowest path loss exponent achieved was 0.45, while the highest path loss exponent was 3.8. We have established that the FI path loss model accurately characterizes path loss for the Lagos Island environment with the lowest RMSE of 0.0359 dB and the highest RSME of 0.0997 dB. In contrast, the CI model over-predict the path loss at 28 GHz with the lowest RMSE of 0.0495 dB and the highest RMSE of 2.2547 dB. This work opens up a new area of research on mm-Wave at 28 GHz in Lagos Island, and the results obtained from this work can be used to benchmark future studies on mmWave in a similar environment.

INDEX TERMS 5G, close-in model, floating intercept model, millimeter-wave, path loss model.

I. INTRODUCTION

The exponential growth in data demand, communication infrastructure, mobile subscription, and high mobile and IoT devices penetration has significantly stretched the cellular bandwidth requirements. Future communication technology needs to improve spectral efficiency, increase the bandwidth and improve the spectrum reuse technology to overcome the current technology limitations. 5G mm-Wave communication promises diverse user applications like smart cities, IoT, industrial automation, and vehicular communication, this is due to its ultra-low latency and massive network capacity associated with higher performance and improved efficiency. Despite the high expectation of 5G, mm-Wave suffers two major drawbacks; high path loss and high penetration losses. The mm-Wave has been shown to operate in extreme power-limited regimes with limited freedom to utilize spatial antenna layout and enhanced bandwidth freedom [1]. Research on adopting artificial neural network (ANN) and deep learning network algorithms like convolutional neural network (CNN) to establish the relationship between the propagation channel features is gaining traction to achieve the expected performance. One possible solution to compensate for the high path loss and penetration losses is to use many antenna elements in a small cell setup. To overcome this challenge, Bao, *et al.* [2] proposed a novel deep CNN model for precoding channel parameters to optimize a combiner neural network architecture aimed at maximizing the spectral efficiency per small cell. The 5G vision is to achieve a flexible radio access scheme supporting massive machine-type communications. 5G mm-Wave communication has been associated with high path loss, high absorption

The associate editor coordinating the review of this manuscript and approving it for publication was Wei Feng.

rate, and critical loss through the foliage. Chen [3] proposed developing a 28 GHz 5G small cell mm-Wave platform to overcome the 5G shortcomings. For optimal location and coverage of transmitter antenna in the mm-Wave network, path loss modeling is crucial. Many approaches have been developed to model path loss using empirical, deterministic, and artificial neural network (ANN) based models. Path loss prediction techniques are valuable tools that can help network optimization engineers deploy base stations, determine base station setup location, transmitting/receiver antenna selection, operating frequency, and interference feasibility studies. Radio propagation models are grouped into empirical and deterministic models. Deterministic models are theoretically based on diffraction principles [4], integral equation [5], ray tracing [6], and parabolic equations [7]. Empirical models are based on drive test measurement of the target areas, examples include; Okumura-Hata [8], standard propagation model [9], and COST 231-Hata model [10]. These models are computationally easy to implement in time and cost-effective. However, they are not as accurate as alternative models as they cannot be adopted for a new environment without adjustment. Cheerla, *et al.* [11] developed an optimized COST 231-Walfisch-Ikegami (CWI) model using Newton's method at frequencies 800 and 1800 MHz. This method proved efficient to accurately predict path loss than the empirical CWI model while validated using actual field measurements. Therefore, it is imperative to study the environment and carry out detailed simulations before conducting a pilot study and implementing the capital-intensive mm-Wave infrastructure. Hence, this research aims to perform a detailed 3D ray-tracing simulation of Lagos Island, Nigeria, at 28 GHz. Erunkulu, *et al.* [12] grouped simulated path loss models into three categories depending on the carrier frequencies, for 28 GHz, the Close-In, Alpha-Beta-Gamma (ABG), and Floating Intercept models are used to characterize path loss at the transmitter to receiver height of 30 m to 2 m respectively. In this work, we present a thorough path loss analysis using CI and FI path loss model at 28 GHz for a transmitter-to-receiver (TR/RX) height of 20/2 m. Other researchers and service providers can adapt the results obtained from this work before implementing 5G network infrastructure to benchmark their study for a similar environment. Table 1 presents the abbreviations and acronyms used in this work. This article aims to develop a new path loss model at 28 GHz specifically tuned to fit Lagos Island's unique terrain comprising high-rise buildings and highly clustered buildings.The objectives of this article are to: (i) Investigate the large-scale path loss effect of Lagos Island at 28 GHz mmWave considering five different scenarios. (ii) Develop a deterministic path loss model using a 3D ray-tracing technique to establish a generic path loss model at 28 GHz to represent South-Western Nigeria. (iii) Calculate the path loss exponent, shadow factor, Mean Absolute Error (MAE), Mean Square Error (MSE), and Root Mean Square Error (RMSE) values to characterize path loss. (iv) Determine the appropriate model amongst Close-In (CI) path loss model and Floating Intercept (FI) path loss model representing Lagos Island. (v) To determine the optimum TX-RX distance to guide the actual implementation of 5G mm-Wave infrastructure.

TABLE 1. Abbreviations and acronyms taxonomy.

Abbreviations	Meaning
3D	Three Dimensional
5G	Fifth Generation
ANN	Artificial Neural Network
BER	Bit Error Rate
CI	Close In
CNN	Convolutional Neural Network
CSV	Comma Separated Values
FI	Floating Intercept
FSPL	Free space path loss
LoS	Line of Sight
LTE	Long Term Evolution
MAE	Mean Absolute Error
mm-Wave	Millimeter-wave
MSE	Mean Square Error
NLoS	Non-LoS
PLE	Path loss exponent
RMSE	Root Mean Square Error
RSS	Receiver Signal Strength
UAV	Unmanned Aerial Vehicle
RX	Receiver
TX	Transmitter
TX1	Transmitter point 1
TX2	Transmitter point 2
TX3	Transmitter point 3
TX4	Transmitter point 4

In this paper, our contributions include; (a) developing a unique deterministic path loss model using the ray-tracing simulation technique at 28 GHz for Lagos Island, Nigeria. The proposed path loss model has been tuned to fit the target environment by calculating the path loss exponent, shadow factor, the random Gaussian standard deviation parameters. (b) Further to this, close-in (CI) and floating intercept (FI) path loss models have been computed for various scenarios to decide the best model to represent large-scale path loss at a 28 GHz environment. (c) Lastly, this work opens up a new area of research on mm-Wave at 28 GHz in Lagos Island and the surrounding environment by using the results obtained in this work to benchmark future works in research, 5G pilot study, and infrastructure implementation. The rest of this paper is organized as follows: Section II discusses the background and related works and depicts a tabular review of key parameters considered in this work. Section III presents the methodology. Section IV presents the results and discusses the results obtained in different scenarios. Section V concludes the article.

II. BACKGROUND AND RELATED WORKS

5G mmWave are associated with high path losses and absorption losses. However, reflection and scattering allow wireless links to be established between the transmitter and receiver in LoS and NLoS. Due to mmWave small wavelength, air and water's molecular size greatly determines the free space achievable across the mmWave spectrum. Temperature and humidity impact the excess attenuation resulting from

absorption. Higher mmWave band suffers from very high excess attenuation over distance. Rappaport, *et al.* [13] attribute the absorption losses to excess path loss caused by oxygen absorption and environmental factors. The excess path loss causes an additional effect on the propagation channel by adding attenuation in the link. The excess path loss for a 60 GHz channel results in an additional 28 dB to the free space path loss. One recommended way to overcome the mmWave path loss is by increasing the antenna size at either the receiver or transmitter. Antenna gain is limited to the effective surface area of the antenna, which directly relates to the permissible path losses. In an LoS mmWave channel, the most effective communication with a directional antenna occurs in the boresight alignment; therefore, the antenna position, location, and pattern affect the communication channel by either increasing the path loss or lowering the path losses. For antennas with a fixed beam pattern, the transmitter should be physically pointed toward the receiver to minimize path losses. In NLoS communication channels, effective communication is best when the antenna pointing is toward one or more dominant reflections within a single beam. The NLoS channel is best when there is a complicated beam pattern that can place energy on multiple propagation paths. The antenna used for NLoS requires some adaptivity to achieve a desirable NLoS channel. Future mmWave antenna should be adaptive with high antenna gain, beamwidth, and beam pointing mechanism to offset and adjust to specific interference levels. Throughout this work, we refer to NLoS environment as path loss scenario, LoS environment as FSPL, which evaluate the effect of antenna pattern on path loss. Hence we consider the case of LoS as FSPL with antenna pattern and FSPL without antenna pattern. The absorption loss is referred to as excess path loss with antenna pattern and excess path loss without antenna pattern. An LoS environment is characterized by a direct non-obstructed path between the transmitter and receiver; an NLoS environment is when the channel has no direct unobstructed path between receiver and transmitter.

Path loss prediction is the ability to forecast the attenuation effect on radio signal propagation with a good level of precision [14]. It is crucial for network planning in wireless communication systems [15]. Extensive field campaigns measuring RSS from the transmitter station to the receiver station helps to generate data needed for propagation path loss determination of a desired wireless network [12], [16]–[18] in a densified cellular network infrastructure [19]. Al-Samman, *et al.* [20] proposed a path loss prediction model for 5G mm-Wave and future 6 GHz wireless communication. The authors developed a new path loss model to account for the path loss associated with 5G networks by introducing a frequency-dependent attenuation factor. Grøtli and Johansen [21] proposed using UAVs for data collection to find the fastest path to solve multi-task missions for direct and multi-hop communication applications. This work concluded that it is possible to improve the propagation signal strength by adopting multiple UAVs for path planning before network infrastructure deployment. Path loss distribution depends on the general characteristics of the area under study[22].

The path loss value depends on the propagation environment; urban, suburban, and rural areas are estimated to have different path loss exponents. An urban environment is estimated to experience a path loss of 30-50 dB generated due to high-rise and other city buildings. The ground terrain is estimated to generate a path loss of 90 dB for every 1 km covered [23]. The effect of path loss on sea and ocean surfaces has been reported by [24], Also, Hrovat, *et al.* [25] research shows that path loss is experienced in tunnels used for metro stations and trains caused by obstacles and traffic in the road and railway tunnel which results to additional signal attenuation, increasing the propagation signal's delay spread. Also, moving objects in the tunnel causes additional path loss accounting for poor communication quality in the tunnel environment. In practice, cellular coverage prediction can be achieved through geometric mathematical models using computer simulations for ray tracing. Using a high computational computer to run cellular coverage prediction saves on time and cost of the incurred drive test. Several vendors have developed 3D modeling software that has been adopted in various works. There are two main models adopted to model path loss prediction: a) drive test measurement campaign, b) propagation simulation modeling using ray tracing and ray launching. In drive test campaigns, sophisticated software and measuring tools are used to measure the propagation characteristics. Presently, ray tracing techniques have been extended to model ANN and CNN-based path loss prediction models by combining 3D models with 2D satellite imagery to develop generic path loss prediction methods [26]–[29] and [30]. While considering 3D digital maps, a given map's accuracy depends on how the terrain, foliage, and city buildings are portrayed; also captured detailed features like building footprints, building edges, facades, street features, vertical and horizontal, and the transmitting and receiving antennas position. Lastly, the path loss prediction by the 3D ray-tracing simulation method offers flexibility and controllability in changing model parameters that are impossible to tune and calibrate in field first-hand practice and serve as a testbed for emulation studies. The main disadvantage of running the 3D ray-tracing simulations is the high computational complexity and time associated with simulations. Ahmadien, *et al.* [26] proposed using 2D satellite image models based on convolutional neural networks to overcome this challenge. Their works showed that path loss distribution could be predicted for wireless networks' various frequencies under varying transmitter and antenna heights. To save on the computational complexity of 3D tracing, Ates, *et al.* [31] proposed a deep learning model using convolutional neural networks (CNNs) with 88% accuracy on path loss exponent and 76% accuracy on large-scale shadowing factor. The author used 3D ray tracing to train and test the model after extracting the relevant features in the 2D satellite images. The deep neural network takes a 2D satellite image as the input and returns a channel parameter prediction. For successful deep learning modeling,

TABLE 2. Taxonomy of related research on path loss modeling parameters at mm-Wave band.

	Model parameters			Close In path loss model			Floating Intercept path loss model	
Ref.	Freq. GHz	TX (m)	RX (m)	Xσ	η, PL	Slope, β	FI,$\alpha(dB)$	SD
[37]	Feb-38	-	-	5.3	2.9	-	-	-
	2.9-73	-	-	8	3.2	-	-	-
[36]	28		-	2.5-10.8	1.7-5.1	0.8-3.7	54.1-94.8	1.6-10.7
	73	-	-	3.2-15.9	1.6-6.4	0.7-2.9	75.6-120.5	2.3-11.7
[42]	19	-	-	-	0.6	-	-	2.4
	28	-	-	-	0.6	-	-	3.3
	38				1.3	-	-	2.4
[43]	28	7	1.5	8.36	3.73	3.73	75.85	-
		17		8.52	4.51	4.51	59.89	-
	38	23	1.5	5.78	3.88	0.12	118.77	-
[44]	3.5	-	-	6.54, 6.97	1.48, 1.95	-	-	-
				5.91, 7.44	1.32, 1.78			
[45]	3.5	-	-	6.98, 7.73,4.99	1.98, 2.07, 1.94	1.92, 4.76, 4.05, 1.27, 3.99, 2.35	37.04, -20.55, -18.13, 50.51, -2.45,24.28	6.89, 7.75, 4.97, 4.87, 5.89, 3.48
				4.89,5.91, 3.50	1.82, 1.99, 1.76			
[46]	28	-	-	4.0, 2.6	2	-	-	-
	38	-	-	2.3, 1.8	2	-	-	-
[47]	40	-	-	4.7, 9.0	1.8, 2.9	1.8, 2.9	70.6, 71.1	7.4, 9.7
[48]	60	-	-	-	1.56-1.78	-	-	-
					3.87			
[49]	28	7;17	15	3.6	2.1	-	-	-
	38	08:36		2.4-3.6	1.8, 1.9, 2.0	-	-	-
	78	7;17	2;4.06	4.2-5.2	2	-	-	-
This study		20	2				See Table 9	

a large dataset is needed for the training and testing set. In 3D modeling, ray tracing is effective in obtaining path loss value and bit error rate (BER). An efficient deep learning model requires massive data to train, test, and validate the model. This data can be generated via a 3D ray-tracing simulation of the target area using propagation modeling software.

Other researchers have applied 3D ray-tracing to model path loss propagation [32]. Charitos, *et al.* [33] adopted a 3D ray-tracing channel to predict the spatial and temporal multipath ray components of radio propagation between an LTE base station and a vehicle. These simulation results are then compared to the actual drive test measurement conducted in the exact area covered by the simulation. This virtual drive test results in higher reliability and repeatability with an accuracy higher than of measured value. The simulation of path loss using a 3D ray-tracing model offers a powerful and cost-effective alternative to on-street drive test campaigns as several parameters can be modeled. Thrane, *et al.* [34] compared the effectiveness of using deep learning techniques utilizing drive test measurement data and satellite images for ray tracing to model path loss models. The developed deep learning model improved path loss prediction with over 1 dB for the cellular network at 811 MHz and 4.7 dB at 2630 MHz. A comprehensive review of the existing path loss model based on the ray-tracing model was done [34]. This review focused on the path loss accuracy achieved by adopting 3D tracing techniques on outdoor propagation scenarios. The authors concluded that digital maps introduce a certain level of uncertainty in the ray tracing models. Still, they offer the best possible and reliable path loss predictions despite the high computational requirements. Han, *et al.* [35] proposed a novel double regression model utilizing an NS-2 simulator that allowed the sender and receiver to move without abrupt changes in the correlated space path loss. The author aimed to overcome the difficulties introduced by sender and receiver in motion by producing spatially correlated path loss in mobile-to-mobile simulation. The model accuracy was validated using drive test campaigns that maintained a spatial correlation of path loss to the empirically observed indoor and outdoor scenarios.

Path loss and atmospheric absorption are significant sources of propagation loss in mm-Wave wireless communication[13]. Maccartney, *et al.* [36], conducted an extensive ultra-wideband mm-Wave propagation measurement campaign at 28 and 73 GHz in New York. This work showed that novel large-scale path loss models are more straightforward and more physically based than previous 3GPP and ITU indoor propagation models. Other similar work by Sun, *et al.* [37] to investigate the prediction accuracy of 5G wireless communication concluded that the alpha-beta-gamma (ABG) model of large-scale path loss model in the microwave and mm-Wave under-predicts path loss, while relatively close to the transmitting antenna and over-predict path loss while far from the transmitter. Further, the results indicated that the physically based two-parameter CI model and three-parameter CIF model offer computational simplicity. In the sequel to this work, Rappaport, *et al.* [38] conducted extensive measurement campaigns for typical base station-to-mobile access scenarios in dense urban environments. This work showed that path loss exponent was immense in a highly populated urban environment like New York City than in Austin. With extensive propagation measurement, it is possible to introduce new path loss models that predict signal strength as a function of distance from the transmitter and the transmission frequency for both indoor and outdoor scenarios. Bhuvaneshwari, *et al.* [39] suggested a hybrid model that combined the Walfisch-Ikegami model and ray-tracing techniques to simulate path loss prediction. This hybrid model reduced the path loss prediction error by 69.9% and relative error by 7.31%. These results was validated by conducting a field campaign in Hyderabad, India, on a GSM 900 MHz

TABLE 3. Taxonomy of related empirical and deterministic path loss models at mm-Wave band.

Ref.	Model	Topology	Environment	Antenna	Freq. (GHz)	T-R (m)	Path loss exponent
[28]	Empirical	NLoS	Suburban	Directional	28	-	1.46-1.60
[29]	Ray tracing	NLoS	Open-square	-	-	-	RMSE 1.5
[42]	Empirical	LoS NLoS	Indoor	Directional	19 28 38	18	0.6 0.6 1.3
[44]	Empirical	LoS NLoS	Indoor	Omnidirectional	3.5	Feb-20	LoS 1.32-1.95 NLoS 1.78
[45]	Empirical	LoS	Outdoor-Rural/Urban	Directional (D*) Omnidirectional (O*)	3.5	60-450	D*=1.98 O*=1.82
[46]	Empirical	LoS NLoS	Outdoor- Campus	Tx -Directional horn Rx-Omni-directional	28 38	14 30	2 2
[47]	Empirical	LoS NLoS	Indoor	Omnidirectional	40	3	1.8 2.9
[48]	Ray tracing	LoS NLoS	Indoor	Omnidirectional	60	-	1.56-1.78 3.78
[50]	Empirical	NLoS	Indoor- Outdoor (I2O)	Omnidirectional	19 28 38	1-13.5	0.4 0.8 1.5
[51]	Empirical	LoS NLoS	Indoor	Directional horn	3.5 28	20	LoS-1.6 NLoS-3.5
[52]	Empirical	LoS NLoS	Indoor	Biconical Dipole	3.5	20	LoS-2-2.5 NLoS-4.1
[53]	Empirical	LoS NLoS	Indoor	Diagonal horn	310 350 390	0.7	2.07 1.9 1.96
[54]	Empirical	LoS NLoS	Outdoor- Urban	Directional horn	38	20-50	3.099 4.3202
[55]	Empirical	LoS	Indoor	Omnidirectional	25.5 28 37.5 39.5	2.54-8.71	0.95 1.02 2.23 2.22
[56]	Empirical	LoS	Indoor	Omnidirectional	2.4 3.52 5.8	4	-
[57]	Empirical	Los	Outdoor	directional	-	28	
[58]	Ray tracing	LoS NLoS	Open-square	-	-	-	RMSE 1.6 10.8
[59]	Ray tracing	LoS	Urban	Isotropic	28	-	-
[60]	Ray tracing	LoS NLoS	Indoor	Omnidirectional	28	-	-
[61]	Ray tracing	LoS NLoS	Outdoor	Omnidirectional	28	-	-
[62]	Empirical and Ray tracing	LoS NLoS	Indoor	Empirical horn 3D-directional	28	22.7	-
This Study	3D Ray tracing	LoS NLoS	Outdoor	Halfwave Dipole	28	See Table 4	See Table 5, Table 6, Table 7, and Table 8

network. Table 2 summarises various research conducted at mm-Wave bands.

The simulation model's performance can be validated with actual field measurement for an urban area, using models like COST-231 Walfish-Ikegami (COST-WI). COST-WI considers the hard to find finite details of the environment like road width, heights of buildings, streets orientations, and foliage, limiting the use of such models in other areas. Other models include COST-231 [10]. Batalha, *et al.* [48] conducted an extensive measurement campaign for an indoor scenario at mm-Wave frequencies. Field measurement data was used to develop a path loss adjusting model through the minimum mean square error (MMSE) method for a close-in path loss model in LoS and NLoS conditions. The author proposed modeling the path loss using 28 GHz frequency for indoor environment, and using the 3D ray-tracing model can achieve this. Degli-Esposti, *et al.* [49] evaluated indoor propagation at mm-Wave by adopting a 3-D ray-tracing model in a small office setup. Using a customized 3D tracing software with three reflections and one transmission, enabled internal office object diffraction and single-bounce diffuse scattering. Later, using the effective roughness model to factor the propagation environment, they considered the best compromise between the accuracy of the results and the central processing unit (CPU) computational requirements. Table 3 represents a taxonomy of related empirical and deterministic path loss models at mm-Wave band.

III. METHODOLOGY

3D ray tracing is a state-of-art deterministic path loss modeling technique. It provides detailed site-specific information necessary to simulate an accurate path loss model [61], [62]. Ray tracing engines offer the flexibility of changing the carrier frequency, transmit, and receiver antennas. In principle,

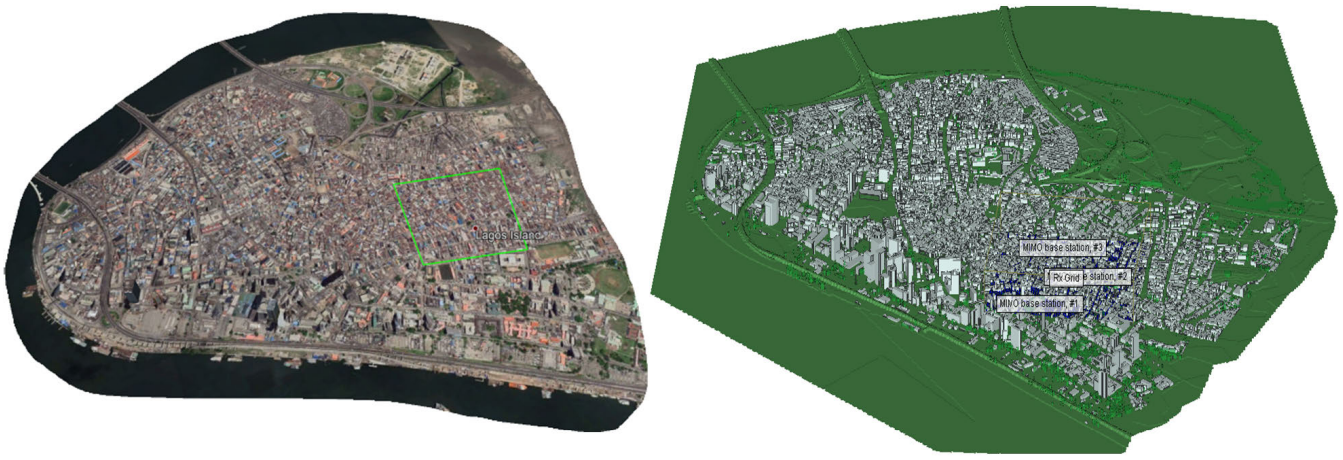

(a) Lagos Island Google Earth Map (b) 3D map of Lagos Island

FIGURE 1. Study area.

deterministic methods offer higher accuracy than empirical models as they are based on geometric optics. Still, the high computational requirement and time required to model path loss is a factor to consider. Ray tracing methods depend on a precise 3D map model of an area of interest encompassing terrain databases, buildings, and foliage databases.

They use an optimization algorithm that calculates the minimum mean square error with the least standard deviation to form the best fit. Ref [57]–[59], [63] proposed a ray tracing simulation technique to model path loss at 28 GHz. Kamboh, *et al.* [64] carried out a 3D ray-tracing at 60 GHz mm-Wave using a simulation model developed in MATLAB. The author used the 5G 3GPP propagation model to compute the received signal strength and path loss. We present a large-scale path loss model at 28 GHz using a 3D map of Lagos Island as a study area, covering coordinates of 6.271735 N to the north, 6.27437 N to the south, 3.235466 E to the southeast, and 3.234122 E to the west. The 28 GHz carrier frequency was preferred for it gives a good tradeoff between unfavorable channel characteristics like path loss, rain fading, propagation loss, transmission through foliage loss, and atmospheric absorption effect. This frequency band has been piloted and implemented in Korea, the US, China, and Japan for the outdoor environment [65]. To achieve high data throughput in a small cell operating on short distances, 28 GHz offers the best carrier frequency [66]. One of the shortcomings of this frequency is susceptibility to high path loss and atmospheric absorption. To overcome the high path loss effect, Karthikeya, *et al.* [67] proposed the design of a co-polarized stacked antenna with a pattern diversity for indoor base stations. Similarly, [68] proposed the use of large-scale antenna arrays to extend the 5G mm-Wave band coverage to lower the effect of path loss. Figure 1 shows the 3D map and the google earth map of the study area. Figure 1(a) depicts the exact position of our study area marked by the green grid bound at coordinates 6.272192/3.234164, 6.271736/3.235836, 6.270134/30235321, and 6.270655/3.233879. The study area covers a distance of 560m with an average elevation of 2.4 m, elevation gain of 11.4m, a maximum slope of 5.7%-8.7%, and an average slope of 1.3%-0.9%.

Figure 2 presents a step-by-step simulation block diagram. First, we imported a 3D map into the software, then the terrain, building, and foliage databases were loaded. For terrain, the material used was dielectric half-space of type ITU dry earth for 28 GHz. The building material considered was a one-layered dielectric of ITU concreate 28 GHz type. The signal waveform applied was a sinusoid, with a carrier frequency of 28 GHz and effective bandwidth of 3000MHz. Four transmitting 30 dBm half-wave dipole antenna with the 28 GHz sinusoid waveform base stations were set up with the coordinates grid edges at the origin longitude of 3.39219575502601 and origin latitude of 6.4562764716583. Receivers were positioned in the XY grid at the height of 2 meters with a spacing of 5 meters.

Figure 3 represents the study grid with the base station and receiver layout and a google map showing the study map. Wireless Insite software runs on several propagation models; amongst them, An X3D study simulation was set to utilize the APG acceleration technique with two diffractions and six reflections on an intel-based Graphic Processing Unit (GPU) workstation running Nvidia GeForce 1050 architecture. The study setup was configured to extract five scenarios of path loss data: path loss, free space path loss with antenna pattern, free space antenna without antenna pattern, excess path loss with antenna pattern, and excess path loss without antenna pattern. Also, other extracted data were received power files, interference and noise data associated with each TX antenna.

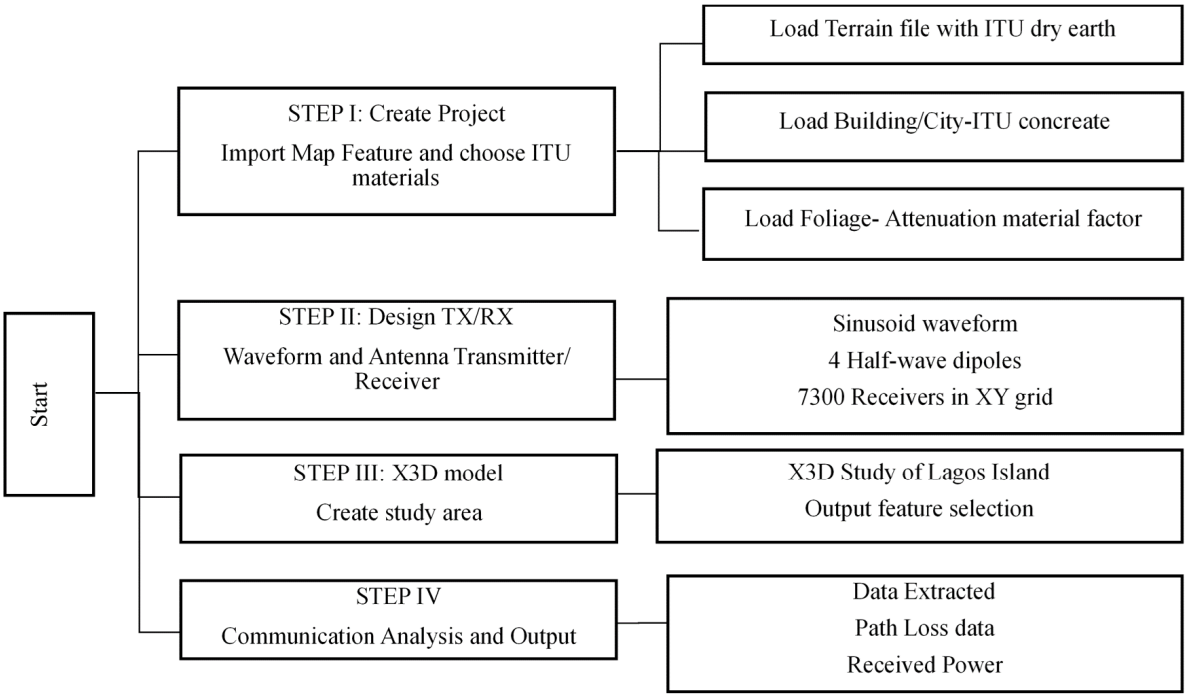

FIGURE 2. Simulation procedure block diagram.

A. SIMULATION SETUP: POINT-TO-MULTIPOINT

In this scenario, the aim was to study the effect of different path loss scenarios in a 5G mm-Wave communication considering the effect of the antenna pattern in the channel throughput and capacity. For this setup, four half-wave dipole transmitter antennas were fixed, as shown in Figure 4. In this scenario, the study focussed on path loss, excess path loss without antenna pattern, excess path loss with antenna pattern, free space path loss without antenna pattern, and free space power without antenna pattern. The TX antennas were labeled TX1, TX2, TX3, TX4, as presented in Figure 4 (b).

Following the steps highlighted in figure 2, the simulation was implemented using a Windows 10 OS, Intel Core i7-8750 H CPU 2.2 GHz, 2208 MHz, 6 Cores, 12 logical processors, Intel Optane+932 GB HDD, and Nvidia GeForce GTX 1050 Graphic Processor with 4 GB dedicated memory. The simulated path loss data were extracted in a text file format and later converted to a CSV file. Table 4 shows the statistical analysis of the simulated path loss data extracted at various transmitter points.

B. 28GHz LARGE SCALE PATH LOSS MODEL FOR URBAN SMALL CELLS ANALYSIS

Path loss is defined as the power loss attenuation between the transmitter and the receiver station[14].i.e.,

PL (dB) = Transmitted power (Pt) dB – Received power (Pr) dB

$$PL\,(dB) = 10log_{10}\left(\frac{Pt}{Pr}\right) \tag{1}$$

where Pt is the power transmitted while Pr is the power received at the close-in reference point.

Free space path loss is a non-negative number defined as the power loss attenuation between the transmitter and the receiver station while path gain is a negative path loss.

$$PL\,(dB) = 10log_{10}\left(\frac{Pt}{Pr}\right) = -10\log_{10} G_t G_r \left(\frac{\lambda}{4\pi R}\right)^2 \tag{2}$$

where, Pr is the power at the receiving antenna, Pt is the output power of the transmitting antenna, G_t, G_r is the gain of the transmitting and receiving antenna respectively, λ is the signal wavelength and R is the distance between the transmitter and receiver.

Free space path loss with antenna pattern scenario is achieved when the antenna pattern is included in the communication system design, the free space loss is calculated from the equation (2) by assuming that the transmitter and receiver antenna polarization match perfectly, the space loss in free space reduces to:

$$L_{FSPL\ with\ AP}(dB) = -10\log_{10}\left(\frac{\lambda^2 G_t G_r}{(4\pi)^2 R^2}\right) \ldots + G_{T,max}(dB\iota) + G_{R,max}(dB\iota) \tag{3}$$

Free space path loss without antenna patterns occurs when the antenna pattern is ignored and an isotropic pattern is assumed, the free space reduces to:

$$L_{FSPL\ without\ AP}(dB) = -10\log_{10} G_t G_r \left(\frac{\lambda}{4\pi R}\right)^2 \tag{4}$$

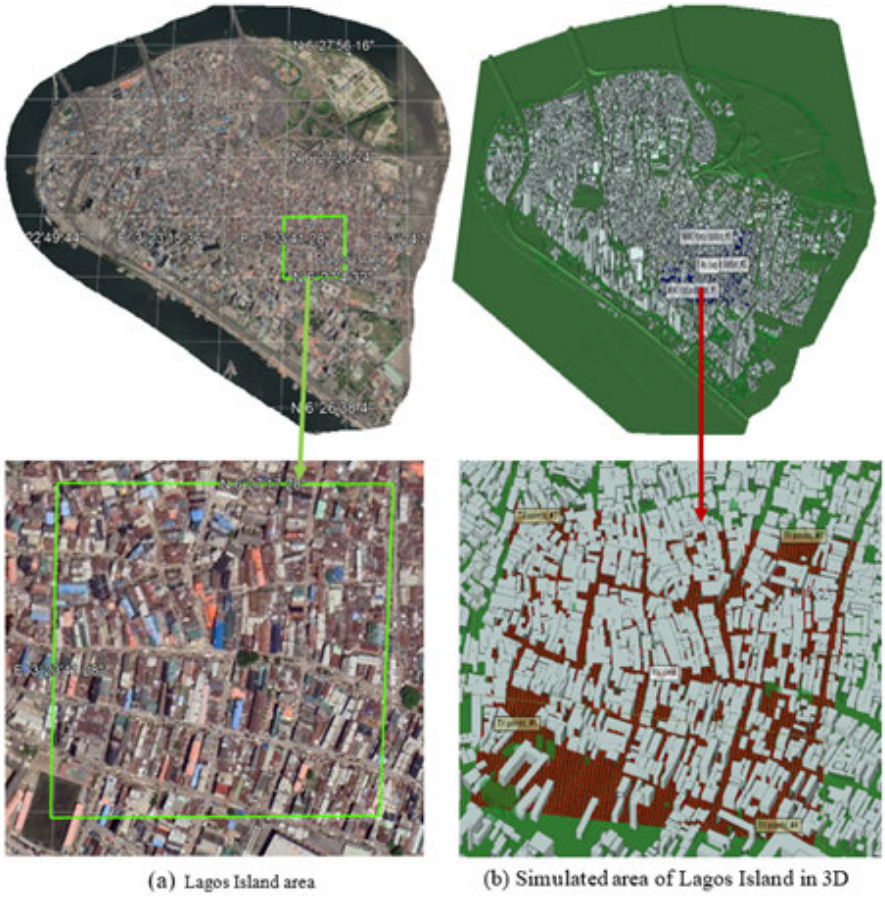

FIGURE 3. Simulated study area.

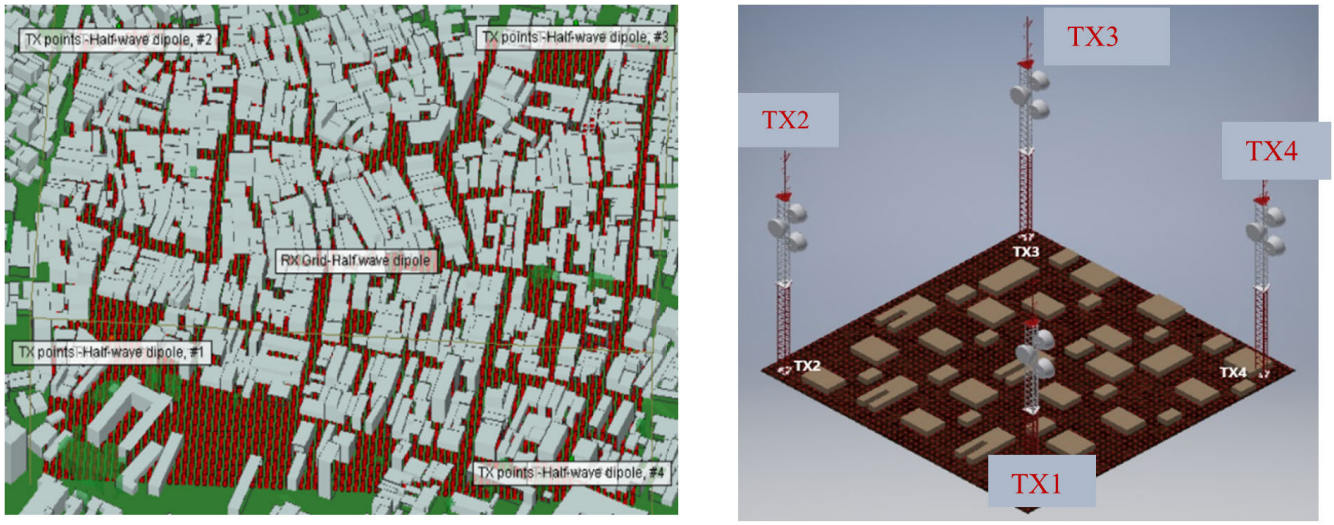

3D simulation antennas position (b) Half-wave dipole TX antennas

FIGURE 4. Point-to-multipoint simulation.

where $L_F SPL$ (dB) is the free space path loss with the antenna patterns. similarly, the excess path loss with antenna pattern scenario is defined as a measure of the loss above that due to free space losses, Its derived as:

$$L_{Excess\ Pl\ with\ AP} = L_{path}(dB) - L_{FSPL\ with\ AP}(dB) \quad (5)$$

TABLE 4. Statistical analysis of the simulated path loss data.

2*Setup	2*Simulation scenario	Statistical analysis of simulated path loss data								
		mean	Std	min	25%	50%	75%	max	skewness	kurtosis
TX 1	Distance	237.86933	108.3813	10.1330	151.2070	244.9545	322.8895	488.2920	-0.10083	-0.89995
	Path loss	215.27657	50.88455	88.6269	169.9420	250.0000	250.0000	253.6810	-1.02428	-0.89995
	FSPL with antenna Pattern	197.7826	70.23602	90.0080	107.07425	250,0000	250.0000	250.0000	-0.60615	-1.62339
	FSPL without Antenna pattern	197.67459	70.39601	81.5099	107.0410	250.0000	250.0000	250.0000	-0.60754	-1.61951
	Excess path loss with antenna pattern	178.36948	98.03095	-18.4442	63.75472	250.0000	250,0000	250.0000	-0.70516	-1.37466
	Excess path loss without antenna pattern	178.47749	97.85613	-4.1855	63.8693	250.0000	250.0000	250.0000	-0.70336	-1.37995
TX 2	Distance	298.74525	120.2263	10.3213	213.2705	312.8250	389.20375	569.1980	-0.30252	-0.59939
	Path loss	238.85283	30.83155	86.5740	250.000	250.0000	250.0000	250.0000	-2.70683	6.293966
	FSPL with antenna Pattern	231.32575	48.79807	90.0065	250.0000	250.0000	250.0000	250.0000	-2.23849	3.035202
	FSPL without Antenna pattern	231.26061	48.98407	81.6698	250.0000	250.0000	250.0000	250.0000	-2.24156	3.055882
	Excess path loss without antenna pattern	225.58127	64.29925	-0.54836	250.0000	250.0000	250.0000	250.0000	-2.30497	3.465721
	Excess path loss with antenna pattern	225.51613	64.49617	-4.3128	250.0000	250.0000	250.0000	250.0000	-2.30897	3.494351
TX 3	Distance	289.43586	117.5947	18.3951	203.6540	301.2220	379.38625	555.0860	-0.23977	-0.71672
	Path loss	207.05964	46.13379	91.9857	164.5405	233.737	250.0000	250.0000	-0.3971	-1.34021
	FSPL with antenna Pattern	178.19465	70.7304	95.5431	109.77225	115.076	250.0000	250.0000	0.025122	-1.98927
	FSPL without Antenna pattern	178.04107	70.90363	86.6903	109.7195	115.0535	250.0000	250.0000	0.023132	-1.98634
	Excess path loss with antenna pattern	151.81301	98.05344	3.08555	54.87375	122.4335	250.0000	250.0000	-0.05138	-1.8956
	Excess path loss without antenna pattern	151.96659	97.85642	-3.08555	54.87375	122.4335	250.0000	250.0000	-0.0483	-1.90134
TX 4	Distance	284.71363	118.2533	18.0011	199.06875	298.129	374.809	552.277	-0.27167	-0.67416
	Path loss	206.4728	50.5878	90.9608	159.84475	250.0000	250.0000	254.019	-0.53625	-1.28534
	FSPL with antenna Pattern	183.53131	71.26561	96.0296	108.81875	250.0000	250.0000	250,0000	-0.14381	-1.97087
	FSPL without Antenna pattern	183.28976	71.55069	86.5022	108.72525	250.0000	250.0000	250.0000	-0.14625	-1.96629
	Excess path loss with antenna pattern	156.49142	101.8082	-51.6886	51.52275	250.0000	250.0000	250.0000	-0.23001	-1.83489
	Excess path loss without antenna pattern	156.73297	101.4989	-8.14919	51.71537	250.0000	250.0000	250.0000	-0.22703	-1.84101

The excess path loss without antenna pattern (dB) is the measure of the loss above that due to the free space without antenna pattern losses. derived as:

$$L_{Excess\ Pl\ without\ AP} = L_{path}(dB) - L_{FSPL\ without\ AP} \quad (6)$$

Also, equation (2) can be extended to factor in the effect of shadowing factor to describe the path loss model at a reference distance d_0.

$$PL\,(d)\,(dB) = PL\,(do) + 10\eta log_{10}\left(\frac{d}{d_0}\right) + X_\sigma \quad (7)$$

where PL(d) represents path loss (dB) at transmitter distance (d), while PL(d_0) is the path loss associated with the reference distance d_0. $X\sigma$ is a random Gaussian variable with zero mean and standard deviation representing shadowing factor in the environment. η is the path loss exponent[69]. In urban areas, shadowing describes the random variable about the distant-dependent large-scale path loss model. This effect is caused by obstruction from buildings, foliage, and other structures, causing random propagation effects. Shadow fading is an essential statistical parameter to model large-scale fading for simulation purposes. It describes the possible path loss value expected while using a distant dependent path loss model without prior knowledge of the site-specific details of an environment. Shadow fading is accurately represented as a log-normal distribution about a distant-dependent mean path loss[69]. Also, path loss can be expressed as:

$$\bar{PL}\,(d)\,(dB) = \alpha + \beta 10log_{10}\,(d) \quad (8)$$

where PL (dB) present the mean path loss over the distances in dB, while α is the floating intercept (FI) in dB. β is the path loss exponent expressed as the linear slope and can be extracted using a best fit linear regression to equation (8), and d represents the TX-TR separation distance. From equations (7) and (8), we can derive shadow factor as:

$$X_\sigma = PL\,(d)\,(dB) - \bar{PL}\,(do) - 10\eta log_{10}\left(\frac{d}{d_0}\right) \quad (9)$$

Similarly, path loss values are calculated from the measured power delay profile (PDPs) by integrating the area under the PDP to obtain the received power at each location and antenna pointing angle. These calculated values are normalized to obtain a channel graph at each antenna pointing combination[41]. The linear slope value β of the path loss exponent η is derived as:

$$\beta = \frac{\sum_i^n \left(d_i - \bar{d}\right) x \left(PL_i - \bar{PL}\right)}{\sum_i^n \left(d_i - \bar{d}\right)^2} \quad (10)$$

where d_i is the separation distance between the antenna and the receiver, d is the average distance of all d_i Values in dB, PLi is the iterated path loss value of all the measured data set as a distance-dependent variable. The floating intercept α (dB) represents the tilt in the path loss model of equation (11). It is calculated by substituting equation (8) into (7) and making α (dB) the subject as in equation (11).

$$\alpha = \bar{PL}\ (dB) + \beta.10\bar{log}_{10}\,(d) \quad (11)$$

The standard deviation σ (dB) (random Gaussian variable) of the path loss models can be calculated as:

$$\sigma\,(dB) = \sqrt{\sum \frac{\left(PL_i - \bar{PL}\right)^2}{N}} \quad (12)$$

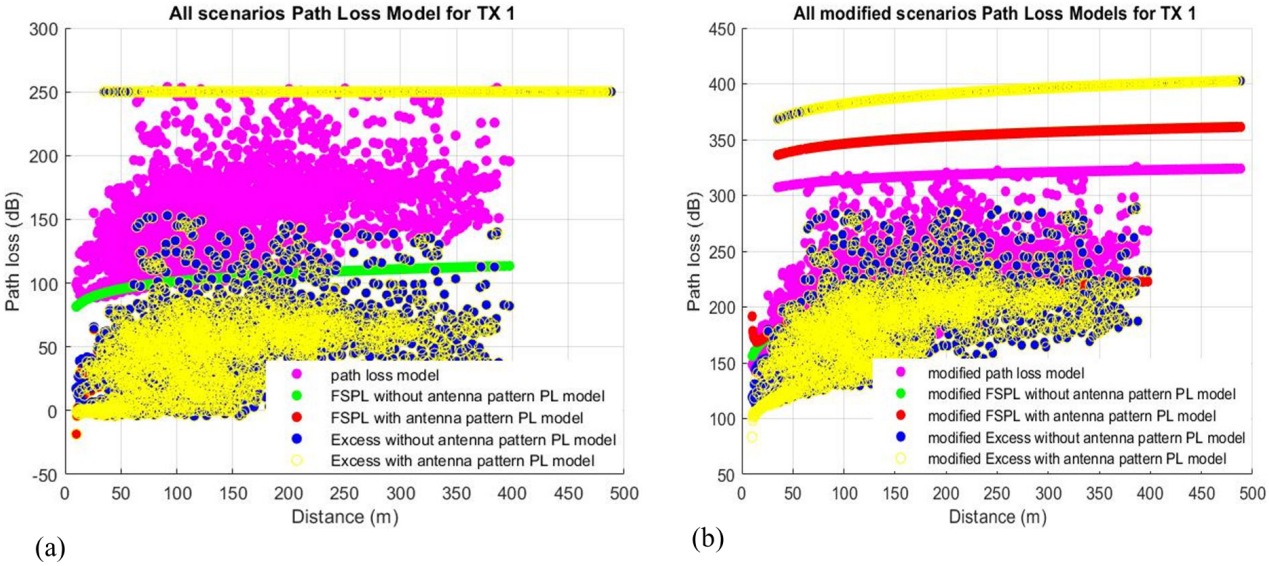

FIGURE 5. Path loss model versus modified path loss models for TX1.

where N is the total number of receiver points in the XY grid, adopting the formulated equations expressed in equation (1) to equation (12). MATLAB was used to model the regression fit for the various path loss scenarios as discussed in Figure 5, Figure 6, Figure 7, and Figure 8

C. ACCURACY EVALUATION OF LARGE SCALE mmWave PATH LOSS MODEL

To evaluate the accuracy of the CI and FI model developed, statistical error for each scenario was calculated using the mean absolute error (MAE), mean square error (MSE), and the root mean square error (RMSE), as shown in the following equations:

$$MAE = \frac{1}{n}\sum_{i=1}^{n}\left(Pl_i^S - Pl_i^P\right) \tag{13}$$

$$MSE = \frac{1}{n}\sum_{i=1}^{n}\left(Pl_i^S - Pl_i^P\right)^2 \tag{14}$$

$$RMSE = \sqrt{\frac{1}{n}\sum_{i=1}^{n}\left(Pl_i^S - Pl_i^P\right)^2} \tag{15}$$

where Pl_i^S denote the simulated path loss measurement, Pl_i present the predicted path loss data using the CI and FI path loss models, and Pl_i^{S-Mean} represents the mean of simulated path loss data.

IV. RESULTS AND DISCUSSION

Large-scale path loss experienced between the transmitter and receiver stations is represented as a function of distance using a path loss exponent value. The acceptable path loss is between 2.7 to 3.5 for urban areas, 3 to 5 for shadowed areas, 2 for in buildings LoS, for obstructed in-building is between 4 to 6, and 2 to 3 for an obstructed environment with factories[69]. For LoS mmWave at 28 GHz, the acceptable path loss is between 1.8 and 2.2 but changes to 4 and 5 in NLoS conditions or LoS when the transmitter and receiver are not in boresight alignment[13]. In this work, the achieved path loss varies between 0.45 dB to 3.8 dB. Lagos Island can be categorized as an urban environment with high-rise buildings causing shadowing and propagation signal obstruction; also, there are a number of large warehouses and factories within Lagos Island, thus fitting the acceptable environment to calculate the path loss exponent from all the scenarios presented in this work, the derived path loss exponent is within the range of acceptable path loss exponent.

Figure 5 presents a path loss model at 28 GHz as a function of the distance between the transmitter at TX1 to the receiver grid. For this scenario, the TX-RX is 10.13 m to 488.292 m. The simulation measures the various path losses associated with the 7300 receivers in the grid. Figure 5(a) represents the path loss scenario data point. In contrast, Figure 5(b) shows the resultant modified path loss model with floating intercept and shadow factor computed to develop a matching path loss model at 28 GHz for Lagos Island. The calculated path loss exponent for path loss, FSPL with antenna pattern, FSPL without antenna pattern, Excess path loss with antenna pattern, Excess path loss without antenna pattern for TX1 were 1.46, 2.1974, 2.2019, 3.0098, and 3.0143, while the corresponding shadow factors were 34.7234, 52.2174, 52.3254, 71.5225 and 71.5225, respectively. The difference in path loss across the 5-scenarios is as discussed in Table 5. The transmitter TX2 was positioned in a highly developed area with multiple high-rise buildings, and some receivers were obstructed from the TX2 line of sight. In this scenario, the magenta color represents the high path loss effect attributed to the high-rise buildings. Figure 6(a) illustrates the

TABLE 5. Transmitter point TX1 key parameters.

TX1 Scenario	Key path loss parameters from equations					
	TR-RX (m) mean	PL (dB) mean	β	FI $\alpha(dB)$	σ	Pl η
Path loss	237.8693	215.2766	0.1387	211.9816	34.7234	1.4612
FSPL with antenna Pattern	237.8693	197.7826	0.2085	192.8275	52.2174	2.1974
FSPL without Antenna pattern	237.8693	197.6746	0.2089	192.7093	52.3254	2.2019
Excess path loss with antenna pattern	237.8693	178.3695	0.286	171.5722	71.6305	3.0098
Excess path loss without antenna pattern	237.8693	178.4775	0.2856	171.6905	71.5225	3.0143

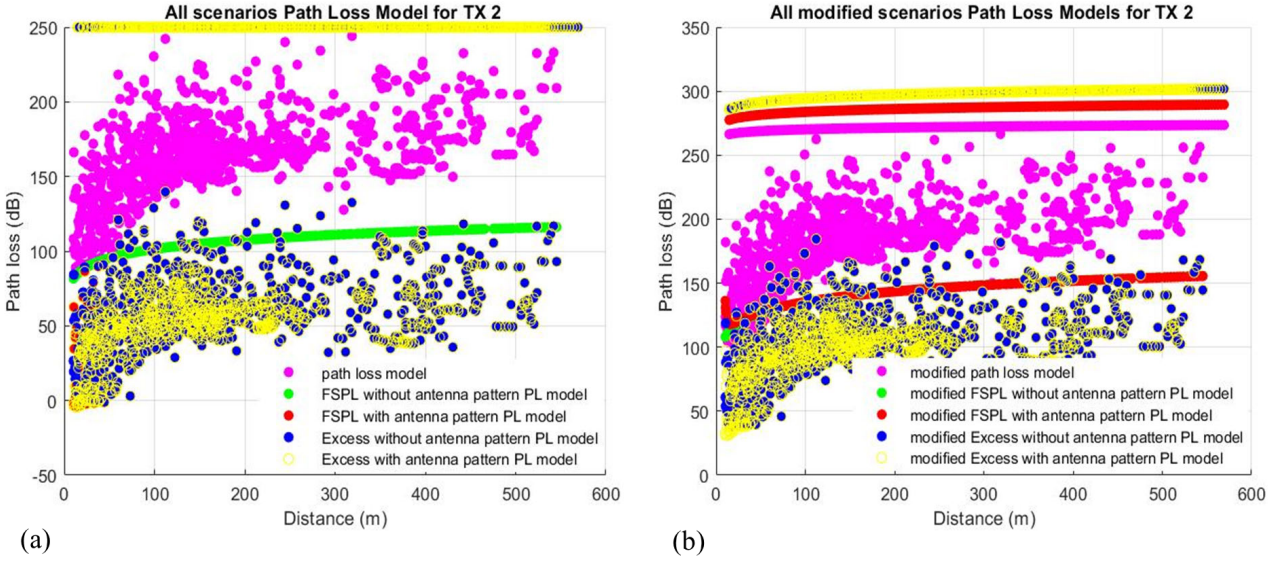

FIGURE 6. Path loss model versus modified path loss models for TX2.

path loss models for TX2. However, the impact of path loss was reduced after modifying equation (4) to introduce the shadow factor, as shown in Figure 6(b).

The path loss exponent for the various models is 0.4503, 0.7544, 0.7571, 0.9891, 0.9865 for path loss, FSPL with antenna pattern, FSPL without antenna pattern, Excess path loss with antenna pattern, Excess path loss without antenna pattern, respectively, while the show factor is 11.1472, 18.6742, 18.7394, 24.4187, 24.4839, respectively. Table 6 presents the parameters for this setup.

Popoola, *et al.* [70], while determining the optimal parameter for an ANN-based path loss prediction model, concluded that the TX-RX distance is a significant parameter. From this work, it can be shown that a receiver in the LoS distance resulted in lower path loss presented in the yellow color of Figure 7 than the NLoS scenario presented in magenta color.

The path loss model represented in Figure 7(a) indicates the simulated value, while Figure 7(b) illustrates the modified path loss model for the various case considered in TX3 as shown in Figure 7. The calculated shadow factor for this scenario were 34.7234, 52.2174, 52.3254, 71.6305, and 71.5225 for path loss, FSPL with antenna pattern, FSPL without antenna pattern, Excess path loss with antenna pattern, Excess path loss without antenna pattern, respectively. The corresponding critical parameters for these scenarios are represented in Table 7.

For transmitter point TX4, the path loss exponent calculated using equation (7) for the various scenarios is 1.7734, 2.0781, 2.7180, 3.8098, and 3.8000, while the shadow factor was 43.5272, 66.4687, 66.7102, 93.5086, and 93.2670 for path loss, FSPL with antenna pattern, FSPL without antenna pattern, Excess path loss with antenna pattern, Excess path loss without antenna pattern. Figure 8(b) shows that the modified path loss model had improved exponent and shadow factor hence the lower path effect. Table 8 represent the TX4 key parameter adopted to develop Figure 8.

1) FI PATH LOSS MODEL AND CI PATH LOSS MODEL ANALYSIS

The FI model is obtained by performing a least square regression of the simulated path loss in the various scenarios. The key parameters for the FI model are (η, β, σ). The CI model is obtained from simulated data by calculating the path loss exponent (η) and shadow factor X_σ.

Figure 9(a) represents the path loss model, the close-in (CI), and the floating intercept (FI) path loss model for TX1. The FI (α, β, σ) parameters are 211.9816, 0.1387, and 0.4061, respectively, while the CI (η, X_σ) parameters

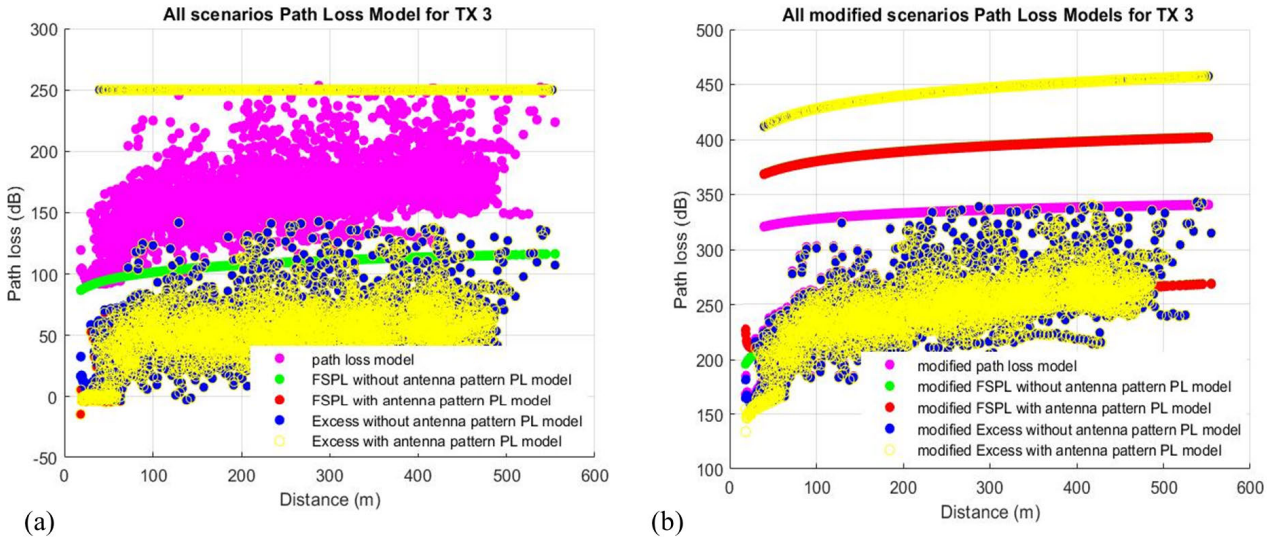

FIGURE 7. Path loss model versus modified path loss models for TX3.

TABLE 6. Transmitter point TX2 key path loss parameters.

TX2 Scenario	Key path loss parameters from equations					
	TR-RX (m) mean	PL (dB) mean	β	FI $\alpha(dB)$	σ	Pl η
Path loss	298.7453	238.8528	0.1135	236.0442	11.1472	0.4503
FSPL with antenna Pattern	298.7453	231.3258	0.1174	231.3258	18.6742	0.7544
FSPL without Antenna pattern	298.7453	231.2606	0.1178	228.3455	18.7394	0.7571
Excess path loss without antenna pattern	298.7453	225.5813	0.2486	219.4289	24.4187	0.9891
Excess path loss with antenna pattern	298.7453	225.5161	0.2492	219.3473	24.4839	0.9865

TABLE 7. Transmitter point TX3 key parameters.

TX3 Scenario	Key path loss parameters from equations					
	TR-RX (m) mean	PL (dB) mean	β	FI $\alpha(dB)$	σ	Pl η
Path loss	237.8693	215.2766	0.1387	211.9816	34.7234	1.744
FSPL with antenna Pattern	237.8693	197.7826	0.2085	192.8275	52.2174	2.9171
FSPL without Antenna pattern	237.8693	197.6746	0.2089	192.7093	52.3254	2.9233
Excess path loss with antenna pattern	237.8693	178.3695	0.286	171.5722	71.6305	3.9888
Excess path loss without antenna pattern	237.8693	178.4775	0.2856	171.6905	71.5225	3.9826

are 1.4612 and 34.7234. similarly, Figure 9(b) represents TX2, the FI (α, β, σ) parameters are 236.0442, 0.1135, and 0.1304, the $CI(\eta, X_\sigma)$ parameters are 0.4503 and 11.1472. Figure 9 (c) shows the TX3 FI (α, β, σ) parameters with 211.8493, -0.1946, and 0.8398 respectively. The CI model for this scenario has an exponent (η) value of 1.744 and a shadow factor of 42.8493. For transmitter point TX4, the CI model and FI model is represented by Figure 9(d), the path loss exponent for this scenario is 1.7734 with a shadow factor of 43.5272, the FI model gives a floating intercept of 197.4515, a standard deviation of 0.5091 and a random gaussian variable of 0.3676. comparing FI and CI models, we conclude that the FI model gives a better approximation of the path loss effect while the CI model increases the path loss.

Table 9 presents a statistical summary of the CI model and FI model key parameters as represented in Figure 5 to Figure 8, showing the simulated path loss model, close-in model, and the floating intercept model for TX1, TX2, TX3, and TX4.

2) MODIFIED AVERAGE FI AND CI PATH LOSS MODELS

According to [14] the average path loss at a distance (d) also called local mean attenuation (LMA) decreases with distance due to the free space path loss and signal obstruction. Path loss model has been represented using CI model and FI model as discussed by [36]–[46], and [47] using equation (1) to equation (7) as discussed in the previous section. From this premise, we develop generic path loss models by taking the average values of each scenario simulated and

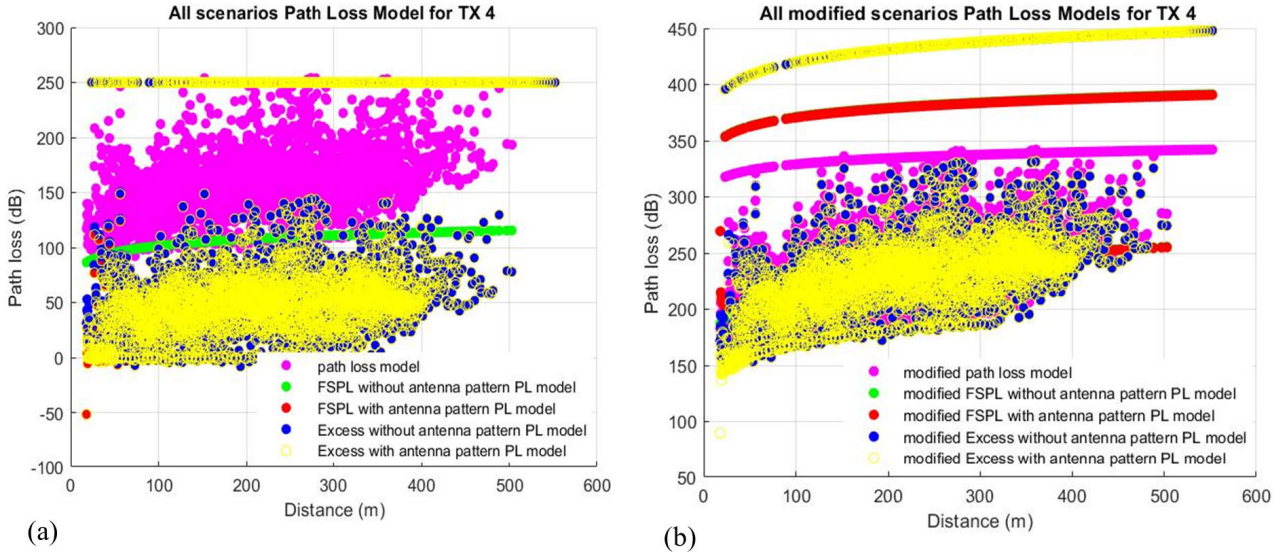

FIGURE 8. Path loss model versus modified path loss models for TX4.

TABLE 8. Transmitter point TX4 key path loss parameters.

TX4 Scenario		Key path loss parameters from equations				
	TR-RX (m) mean	PL (dB) mean	β	FI $\alpha(dB)$	σ	Pl η
Path loss	284.7136	206.4728	0.3676	197.4515	43.5272	1.7734
FSPL with antenna Pattern	284.7136	183.5313	0.5613	169.7552	66.4687	2.7081
FSPL without Antenna pattern	284.7136	183.2898	0.5633	169.4636	66.7102	2.718
Excess path loss with antenna pattern	284.7136	156.4914	0.7896	137.1111	93.5086	3.8098
Excess path loss without antenna pattern	284.7136	156.733	0.7876	137.4027	93.267	3.8

TABLE 9. Summary of the CI model and FI model key parameters.

Setup	Scenario	Close In Model		Floating Intercept Model		
		η	Xσ	α	β	σ
TX1	Path loss	1.4612	34.7234	211.9816	0.1387	0.4061
	FSPL with antenna Pattern	2.1974	52.2174	192.8275	0.2085	0.6107
	FSPL without Antenna pattern	2.2019	52.3254	192.7093	0.2089	0.612
	Excess path loss with antenna pattern	3.0098	71.6305	171.5722	0.286	0.8378
	Excess path loss without antenna pattern	3.0143	71.5225	171.6905	0.2856	0.8365
TX2	Path loss	0.4503	11.1472	236.0442	0.1135	0.1304
	FSPL with antenna Pattern	0.7544	18.6742	231.3258	0.1174	0.2184
	FSPL without Antenna pattern	0.7571	18.7394	228.3455	0.1178	0.2192
	Excess path loss without antenna pattern	0.9891	24.4187	219.4289	0.2486	0.2864
	Excess path loss with antenna pattern	0.9865	24.4839	219.3473	0.2492	0.5022
TX4	Path loss	1.744	42.9404	211.8493	-0.1946	0.8398
	FSPL with antenna Pattern	2.9171	71.8053	186.2039	-0.3254	0.8416
	FSPL without Antenna pattern	2.9233	71.9589	186.0675	-0.3261	1.1484
	Excess path loss with antenna pattern	3.9888	98.0334	162.9014	-0.4442	1.1466
	Excess path loss without antenna pattern	3.9826	98.1870	162.7649	-0.4449	0.5022
TX4	Path loss	1.7734	43.5272	197.4515	0.3676	0.5091
	FSPL with antenna Pattern	2.7081	66.4687	169.7552	0.5613	0.7774
	FSPL without Antenna pattern	2.7180	66.7102	169.4636	0.5633	0.7802
	Excess path loss with antenna pattern	3.8098	93.5086	137.1111	0.7896	1.0937
	Excess path loss without antenna pattern	3.8000	93.2670	137.4027	0.7876	1.0909

representing TX1, TX2, TX3, and TX4 as a single value, as shown in Table 10.

For a CI model, we use the average value for η and X_σ to calculate a regression fitting model to develop

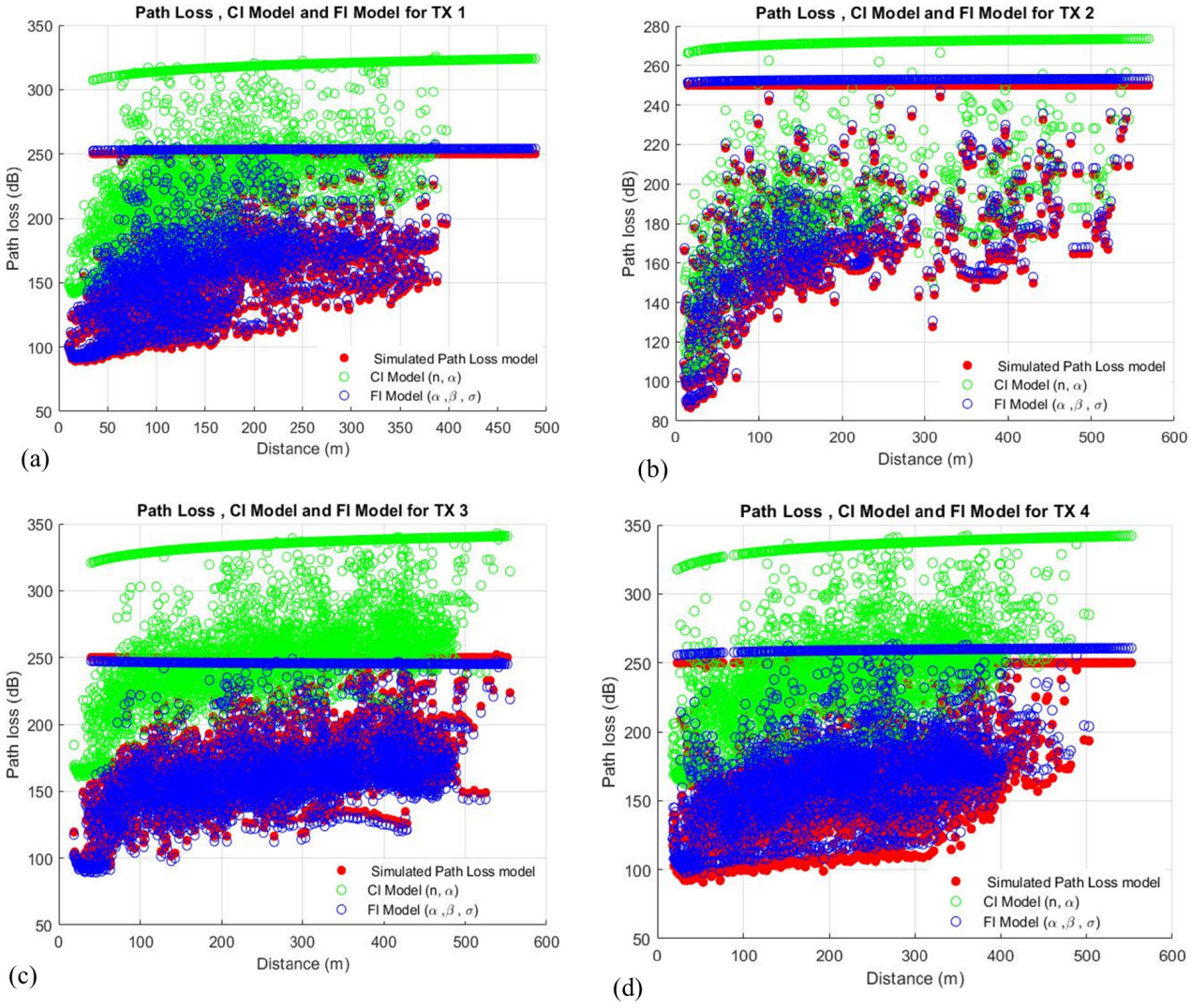

FIGURE 9. Path loss model, CI, and FI path loss model for all TX points.

TABLE 10. Modified average CI and FI path loss model.

Setup	Scenario	TX-RX (m)	PL (dB)	Close In (CI) Model		Floating Intercept (FI) Model		
				n	shadow	alpha	beta	F Intercept
Path loss scenarios	TX1	237.8693	193.51616	2.37692	56.48384	188.15622	0.22554	0.66062
	TX2	298.8693	276.82358	0.78748	19.18052	226.89834	0.1693	0.27132
	TX3	289.4359	173.59856	3.11116	76.5850	181.9574	-0.34704	0.89572
	TX4	284.7136	177.30366	2.96186	72.69634	162.6820	0.6138	0.85026
Average of all TX points		277.722	205.31049	2.309355	56.236425	189.92352	0.1654	0.66948

equation (16)

$$(PL)^{CI}\, dB = PL\,(d)\,(dB) + 10.\eta.log_{10}\,(d) + X_\sigma{}^{CI} \quad (16)$$

where PL(d) dB is the average path loss at each transmission station, η is the average path loss exponent, d is the average distance between the transmitter and the receiver point, and $X\sigma$ is the average shadow factor for the transmitter points. Taking the average CI parameters and substituting them in equation (16) results in a new CI path loss model for Lagos Island at 28 GHz. PL(d) dB is the average path loss for corresponding TX points as shown from equation (17) to equation (20)

$$TX1_C I \;=\; \mathbf{250} + \mathbf{23.7692}log_{\mathbf{10}}\,(d) \quad (17)$$

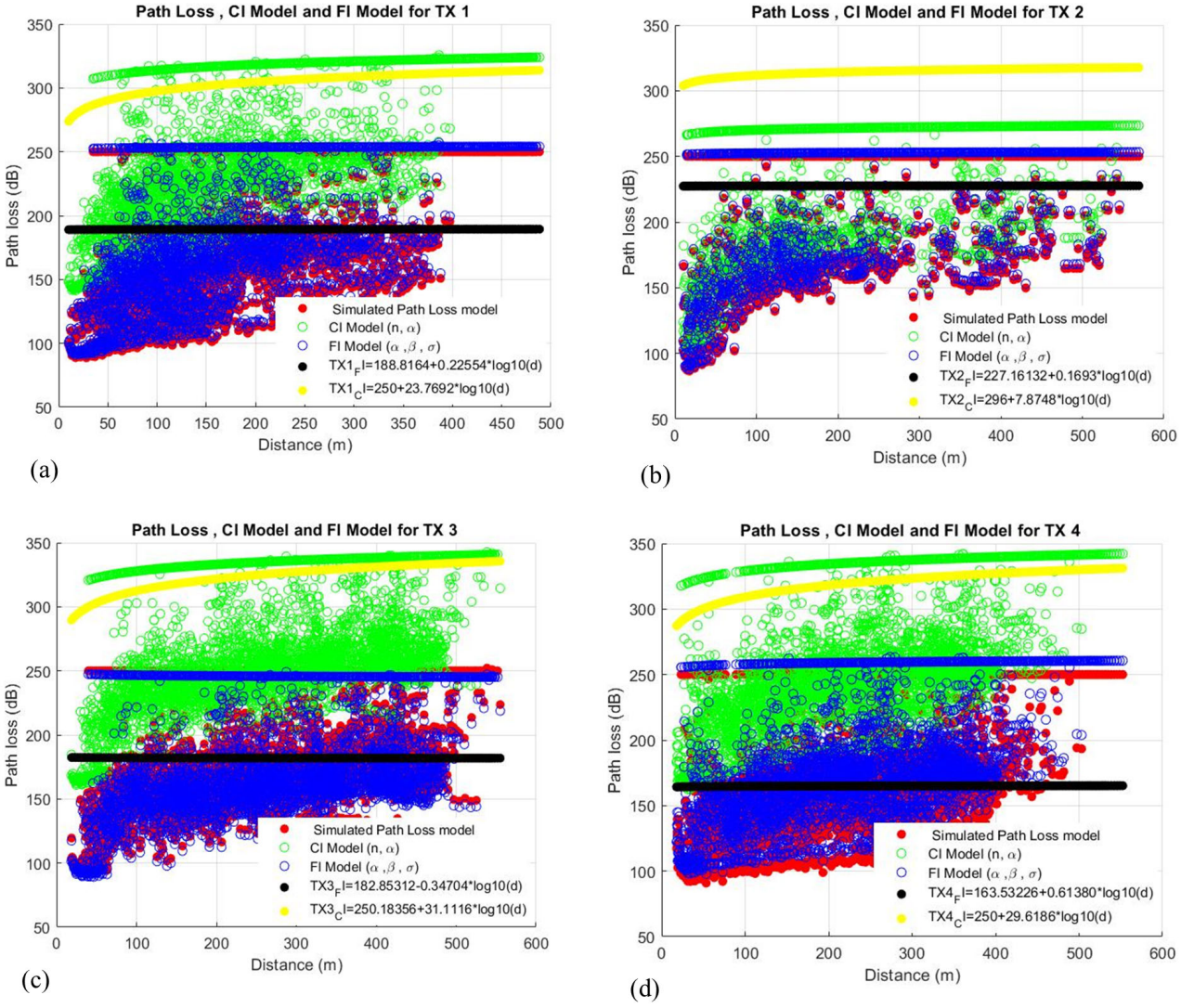

FIGURE 10. Average modified CI and FI path loss models.

$$TX2_CI = \mathbf{296.0041} + \mathbf{7.8748}log_{\mathbf{10}}(d) \quad (18)$$

$$TX3_CI = \mathbf{250.18356} + \mathbf{31.1116}log_{\mathbf{10}}(d) \quad (19)$$

$$TX4_CI = \mathbf{250} + \mathbf{29.6186}log_{\mathbf{10}}(d) \quad (20)$$

For the FI model, we compute the average values as represented in Table 10 to develop equation (21) as:

$$(PL)^{FI}\, dB = \alpha + \beta^{FI}.10.log_{10}(d) + \sigma^{FI} \quad (21)$$

where PL (dB) is the developed path loss model, α gives the average floating intercept value of the transmission points, β^{FI} represent the average slope of the TX scenario points and σ^{FI} represent the average random Gaussian parameter expressed as a standard deviation of the Gaussian random variable of the simulated data. For each transmitter point, this is calculated as shown in equation (22) to (25):

$$TX1_FI = \mathbf{188.81684} + \mathbf{0.22554}log_{\mathbf{10}}(d) \quad (22)$$

$$TX2_FI = \mathbf{227.16132} + \mathbf{0.1693}log_{\mathbf{10}}(d) \quad (23)$$

$$TX3_FI = \mathbf{182.85312} - \mathbf{0.34704}log_{\mathbf{10}}(d) \quad (24)$$

$$TX4_FI = \mathbf{163.53226} + \mathbf{0.61380}log_{\mathbf{10}}(d) \quad (25)$$

Figure 10 shows the corresponding plots of the developed CI and FI path loss model. The newly defined CI model and FI models show the optimal path loss for each transmitter point.

3) PERFORMANCE EVALUATION OF THE LARGE SCALE mmWAVE PATH LOSS MODEL

The prediction accuracy of the path loss model is evaluated using the RMSE. The best performance is exhibited when the RMSE values are close to 0 dB. However, the acceptable RMSE values for urban areas are 6-7 dB, while suburban areas range between 10-15 dB [69]. Table 11, Table 12, Table 13, and Table 14 represent the statistical error evaluation value for the simulated data against the CI and FI path loss model developed for TX1, TX2, TX3, and TX4. The RMSE value for the TX1 path loss was 0.4061 dB, while the

TABLE 11. Path loss performance evaluation.

Scenarios	PL models	MAE	MSE	RMSE
Path loss	Simulated	0.0048	0.1649	0.4061
	Close-In	0.0101	0.7493	0.8656
	Floating Intercept	5.66E-04	0.0023	0.0484
FSPL without antenna pattern	Simulated	0.0072	0.3745	0.612
	Close-In	0.0153	1.7016	1.3044
	Floating Intercept	8.12E-04	0.005	0.0705
FSPL with antenna pattern	Simulated	0.0071	0.373	0.6107
	Close-In	0.0152	1.6946	1.3018
	Floating Intercept	8.50E-04	0.0053	0.0727
Excess path loss without antenna pattern	Simulated	0.0098	0.6998	0.8365
	Close-In	0.0209	3.1792	1.783
	Floating Intercept	0.0012	0.0096	0.0996
Excess path loss with antenna pattern	Simulated	0.0098	0.7019	0.8378
	Close-In	0.0209	3.1888	1.7857
	Floating Intercept	0.0012	0.01	0.0997

TABLE 12. TX2 path loss performance evaluation.

Scenarios	PL models	MAE	MSE	RMSE
Path loss	Simulated	0.0015	0.017	0.1304
	Close-In	0.0031	0.0714	0.2673
	Floating Intercept	4.21E-04	0.0013	0.036
FSPL without antenna pattern	Simulated	0.0026	0.048	0.2192
	Close-In	0.0053	0.2019	0.4493
	Floating Intercept	6.96E-04	0.0035	0.0595
FSPL with antenna pattern	Simulated	0.0026	0.0477	0.2184
	Close-In	0.0052	0.2005	0.4477
	Floating Intercept	7.06E-04	0.0036	0.0603
Excess path loss without antenna pattern	Simulated	0.0033	0.8016	0.2856
	Close-In	0.0068	0.3428	0.5855
	Floating Intercept	9.23E-04	0.0062	0.0789
Excess path loss with antenna pattern	Simulated	0.0033	0.082	0.2864
	Close-In	0.0069	0.3446	0.587
	Floating Intercept	9.25E-04	0.0063	0.0791

TABLE 13. TX3 path loss performance evaluation.

Scenarios	PL models	MAE	MSE	RMSE
Path loss	Simulated	0.0059	0.2522	0.5022
	Close-In	0.0103	0.7693	0.8771
	Floating Intercept	4.20E-04	0.0013	0.0359
FSPL without antenna pattern	Simulated	0.0098	0.7084	0.8416
	Close-In	0.0172	2.1604	1.4698
	Floating Intercept	7.51E-04	0.0041	0.0642
FSPL with antenna pattern	Simulated	0.0098	0.7053	0.8398
	Close-In	0.0172	2.1512	1.4667
	Floating Intercept	7.03E-04	0.0036	0.0601
Excess path loss without antenna pattern	Simulated	0.0134	1.3147	1.1466
	Close-In	0.0234	1.3147	1.1466
	Floating Intercept	9.60E-04	0.0067	0.082
Excess path loss with antenna pattern	Simulated	0.0134	1.3188	1.1484
	Close-In	0.0235	4.0223	2.0056
	Floating Intercept	9.61E-04	0.0068	0.0822

TABLE 14. TX4 path loss performance evaluation.

Scenarios	PL models	MAE	MSE	RMSE
Path loss	Simulated	0.006	0.2592	0.5091
	Close-In	0.0123	1.1015	1.0495
	Floating Intercept	0.0014	0.0139	0.118
FSPL without antenna pattern	Simulated	0.0091	0.6088	0.7802
	Close-In	0.0188	2.5873	1.6085
	Floating Intercept	0.0021	0.0315	0.1776
FSPL with antenna pattern	Simulated	0.0091	0.6044	0.7774
	Close-In	0.0187	2.5686	1.6027
	Floating Intercept	0.0021	0.0324	0.1801
Excess path loss without antenna pattern	Simulated	0.0128	1.19	1.0909
	Close-In	0.0263	5.0573	2.2489
	Floating Intercept	0.003	0.0639	0.2528
Excess path loss with antenna pattern	Simulated	0.0128	1.1961	1.0937
	Close-In	0.0264	5.0836	2.2547
	Floating Intercept	0.003	0.0642	0.2534

CI resulted in 0.8656 dB, and the FI model had 0.0484. For FSPL without antenna pattern and FSPL with antenna pattern, the RMSE values are 1.3044dB, 1.3018 dB for the CI model, and 0.0705 dB and 0.0727 dB for the FI model. The RMSE value for the excess path loss with antenna pattern and excess path loss without antenna pattern is 1.7830 dB and 1.7857 dB for the CI model and 0.0996 dB and 0.0997 dB for the FI path loss model.

For transmitter TX2, the simulated path loss RMSE value CI had 0.2673 dB. The FI model had 0.0360 dB, the FSPL with antenna pattern, FSPL without antenna pattern, excess path loss without antenna pattern, and excess path loss with antenna pattern had 0.4493 dB, 0.4477 dB, 0.5855 dB, and 0.5870 dB for the CI model. In comparison, the FI model had 0.0595 dB, 0.0603 dB, 0.0789 dB, and 0.0791 dB for the FI model. Table 12 presents the MAE, MSE, and RMSE for TX2 scenarios.

The RMSE values for the CI model at TX3 were 0.8771 dB, 1.4698 dB, 1.4667 dB, 1.1466 dB, and 2.0056 dB for the path loss, FSPL without antenna pattern, FSPL with antenna pattern, excess path loss without antenna pattern, and the excess path loss with antenna pattern, respectively. The FI model had 0.0359 dB, 0.0642 dB, 0.0601 dB, 0.0820 dB and 0.0822 dB as presented in Table 13.

In Table 14, the FI model had 0.1180 dB, 0.1776 dB, 0.1801 dB, 0.2528 dB, and 0.2534 dB for path loss, FSPL without antenna pattern, FSPL with antenna pattern, excess path loss without antenna pattern, and for the excess path loss with antenna pattern, respectively. The CI model had 1.0495 dB, 1.6085 dB, 1.6027 dB, 2.2489 dB, and 2.2547 dB for the scenarios presented in Table 14.

Comparing the CI and FI model RSME values for all scenarios, the FI path loss scenario had the lowest RMSE of 0.0484 dB, 0.036 dB, 0.0359 dB, 0.1180dB for TX1, TX2, TX3, and TX4. In comparison, the excess path loss with antenna pattern resulted in the highest RMSE of 0.0997 dB, 0.0791 dB, 0.0822 dB, and 0.2534 dB, respectively. The CI model had RMSE value of 0.8656 dB, 0.2673 dB, 0.8771 dB, and 0.0495 dB for TX1, TX2, TX3, and TX4. The highest RMSE value for the CI model was under the excess path loss with antenna scenarios with 1.7857 dB, 0.5870 dB, 2.0056 dB, and 2.2547 dB for the TX1, TX2, TX3, and TX4, respectively. Table 11, Table 12, Table 13, and Table 14 show that the FI model had the smallest RMSE value (dB) than the CI model for all the scenarios across all TXs. This signifies that the FI model gives the best path loss prediction across all the scenarios considered in this work. The CI model had a considerably higher RMSE value(s) (dB) in all cases.

Therefore it overpredicted the corresponding path losses in all the considered scenarios. Hence, we report that for Lagos Island, the FI path loss model accurately predicts path loss at 28 GHz for a transmitter height of 20 m and receiver height of 2 m.

Comparing the path loss models presented by [36], [37], [40], [41], [44], and [47] with our path loss model, our model shows an optimistic advantage over all reviewed pieces of literature. Our research conducted a large-scale path loss modeling. The simulation model was configured to consider the path loss at any receiver point in the XY grid from the four-transmitter station, the path loss exponent for all the scenarios presented here is with an exponent of 0.45 at TX2, the highest path loss exponent factor was 3.8 at TX4 under the excess path loss with antenna pattern scenario. Ref. [40] model of 28 GHz resulted to a path loss of 0.6 which is higher than our lowest path loss exponent. Ref. [41] reported a path loss exponent of 4.51 at a transmitter height of 17 meters and a receiver height of 1.5 meters. Our model's highest path loss exponent is 3.9888 at Excess path loss with antenna pattern in TX3 at a transmitter height of 20 meters and 2 meters for the receiver grid. The average path loss exponent from all our simulation scenarios is 2.309355, which is less than reported by [36], [41] and [52]. Maccartney, *et al.* [36] achieved a shadow factor of 10.8 at 28 GHz for the close-in path loss model; this work achieved a shadow factor of 11.1472 with a corresponding linear slope of 0.1135, which is less than achieved by [43] and [45] at mmWave frequency. From the figures presented in this research, the FI model accurately fits the simulated environment, while the CI model gives a pessimistic representation of the study area. The results obtained from this work align with the standard path loss model developed by [36], [40], and [41]. Comparing this work with research done at different mm-Wave band presented in Table 2 shows that this work can be adopted by researcher considering to study path loss in Lagos Island in the 2-73 GHz band.

V. CONCLUSION

Large-scale path loss modeling in the mm-Wave band requires calibration and tuning for the case of the field campaign. This work adopted a 3D ray-tracing deterministic method to model a 5G communication testbed for Lagos Island, Nigeria, using Remcom ray tracing suite, Wireless Insite engine. To the best of our knowledge, no similar work has been carried out in the study area at 28 GHz, making this research relevant to 5G communication service providers intending to carry pilot study or actual implementation and other researchers in this domain. From the CI/FI model analysis, we have established that the FI model has the lowest RMSE value (dB) than the CI model for the scenarios considered and exhibits the best prediction model to perfectly characterize the Lagos Island environment. Lagos Island is an urban area comprising high-rise buildings and highly populated areas; it is necessary to investigate how shadow fading affects the path loss models in such an environment. The shadow factor presented in our model depicts an advantaged model compared to other existing research work done at 28 GHz. This model can guide other researchers working in the mm-Wave band for Lagos Island and can be adapted to other areas. For future work, an actual field campaign at 28 GHz in both LoS and NLoS scenarios with and without antenna patterns will be carried out. Also, a similar study will be conducted to cover the four geographical regions in Nigeria.

REFERENCES

[1] M. R. Akdeniz, Y. Liu, S. Rangan, and E. Erkip, "Millimeter wave picocellular system evaluation for urban deployments," in *Proc. IEEE Globecom Workshops*, Dec. 2013, pp. 105–110.
[2] X. Bao, W. Feng, J. Zheng, and J. Li, "Deep CNN and equivalent channel based hybrid precoding for mmWave massive MIMO systems," *IEEE Access*, vol. 8, pp. 19327–19335, 2020.
[3] W. C. Chen, "5G mmWAVE technology design challenges and development trends," in *Proc. Int. Symp. VLSI Design, Autom. Test (VLSI-DAT)*, Aug. 2020, pp. 1–4.
[4] R. J. Luebbers, "Propagation prediction for hilly terrain using GTD wedge diffraction," *IEEE Trans. Antennas Propag.*, vol. AP-32, no. 9, pp. 951–955, Sep. 1984.
[5] G. A. Hufford, "An integral equation approach to the problem of wave propagation over an irregular surface," *Quart. Appl. Math.*, vol. 9, no. 4, pp. 391–404, 1952.
[6] V. Mohtashami and A. Shishegar, "Modified wavefront decomposition method for fast and accurate ray-tracing simulation," *IET Microw., Antennas Propag.*, vol. 6, no. 3, pp. 295–304, 2012.
[7] C. A. Zelley and C. C. Constantinou, "A three-dimensional parabolic equation applied to VHF/UHF propagation over irregular terrain," *IEEE Trans. Antennas Propag.*, vol. 47, no. 10, pp. 1586–1596, Oct. 1999.
[8] M. Hatay, "Empirical formula for propagation loss in land mobile radio services," *IEEE Trans. Veh. Technol.*, vol. VT-29, no. 3, pp. 317–325, Aug. 1980.
[9] S. I. Popoola and O. F. Oseni, "Performance evaluation of radio propagation models on GSM network in urban area of Lagos, Nigeria," *Int. J. Sci. Eng. Res.*, vol. 5, no. 6, pp. 1212–1217, 2014.
[10] R. V. Akhpashev and A. V. Andreev, "COST 231 Hata adaptation model for urban conditions in LTE networks," in *Proc. 17th Int. Conf. Young Specialists Micro/Nanotechnol. Electron Devices (EDM)*, Jun. 2016, pp. 64–66.
[11] S. Cheerla, D. Venkata Ratnam, and J. R. K. K. Dabbakuti, "An optimized path loss model for urban wireless channels," in *Microelectronics, Electromagnetics and Telecommunications*. Singapore: Springer, 2021, pp. 293–301.
[12] O. O. Erunkulu, A. M. Zungeru, C. K. Lebekwe, and J. M. Chuma, "Cellular communications coverage prediction techniques: A survey and comparison," *IEEE Access*, vol. 8, pp. 113052–113077, 2020.
[13] T. S. Rappaport, R. W. Heath, Jr., R. C. Daniels, and J. N. Murdock, *Millimeter Wave Wireless Communications*. London, U.K.: Pearson, 2015.
[14] A. Goldsmith, *Wireless Communications*. Cambridge, U.K.: Cambridge Univ. Press, 2005.
[15] C. Phillips, D. Sicker, and D. Grunwald, "A survey of wireless path loss prediction and coverage mapping methods," *IEEE Commun. Surveys Tuts.*, vol. 15, no. 1, pp. 255–270, 1st Quart., 2013.
[16] M. N. Hindia, A. M. Al-Samman, T. A. Rahman, and T. M. Yazdani, "Outdoor large-scale path loss characterization in an urban environment at 26, 28, 36, and 38 GHz," *Phys. Commun.*, vol. 27, pp. 150–160, Apr. 2018.
[17] S. I. Popoola, A. A. Atayero, and O. A. Popoola, "Comparative assessment of data obtained using empirical models for path loss predictions in a university campus environment," *Data Brief*, vol. 18, pp. 380–393, Jun. 2018.
[18] L. C. Fernandes and A. J. M. Soares, "Path loss prediction in microcellular environments at 900MHz," *AEU-Int. J. Electron. Commun.*, vol. 68, no. 10, pp. 983–989, Oct. 2014.
[19] K. Shehzad, N. M. Khan, and J. Ahmed, "Performance analysis of coverage-centric heterogeneous cellular networks using dual-slope path loss model," *Comput. Netw.*, vol. 185, Feb. 2021, Art. no. 107672.

[20] A. M. Al-Samman, T. A. Rahman, M. H. Azmi, and M. N. Hindia, "Large-scale path loss models and time dispersion in an outdoor line-of-sight environment for 5G wireless communications," *AEU-Int. J. Electron. Commun.*, vol. 70, no. 11, pp. 1515–1521, Nov. 2016.

[21] E. I. Grotli and T. A. Johansen, "Task assignment for cooperating UAVs under radio propagation path loss constraints," in *Proc. Amer. Control Conf. (ACC)*, Jun. 2012, pp. 3278–3283.

[22] V. S. Anusha, G. K. Nithya, and S. N. Rao, "A comprehensive survey of electromagnetic propagation models," in *Proc. Int. Conf. Commun. Signal Process. (ICCSP)*, Apr. 2017, pp. 1457–1462.

[23] T. K. Sarkar, M. N. Abdallah, and M. Salazar-Palma, "Survey of available experimental data of radio wave propagation for wireless transmission," *IEEE Trans. Antennas Propag.*, vol. 66, no. 12, pp. 6665–6672, Dec. 2018.

[24] P. A. S. Balkees, K. Sasidhar, and S. Rao, "A survey based analysis of propagation models over the sea," in *Proc. Int. Conf. Adv. Comput., Commun. Informat. (ICACCI)*, Aug. 2015, pp. 69–75.

[25] A. Hrovat, G. Kandus, and T. Javornik, "A survey of radio propagation modeling for tunnels," *IEEE Commun. Surveys Tuts.*, vol. 16, no. 2, pp. 658–669, 2nd Quart., 2014.

[26] O. Ahmadien, H. F. Ates, T. Baykas, and B. K. Gunturk, "Predicting path loss distribution of an area from satellite images using deep learning," *IEEE Access*, vol. 8, pp. 64982–64991, 2020.

[27] H. Cheng, H. Lee, and S. Ma, "CNN-based indoor path loss modeling with reconstruction of input images," in *Proc. Int. Conf. Inf. Commun. Technol. Converg. (ICTC)*, Oct. 2018, pp. 605–610.

[28] H. Cheng, S. Ma, and H. Lee, "CNN-based mmWave path loss modeling for fixed wireless access in suburban scenarios," *IEEE Antennas Wireless Propag. Lett.*, vol. 19, no. 10, pp. 1694–1698, Oct. 2020.

[29] N. Kuno, W. Yamada, M. Sasaki, and Y. Takatori, "Convolutional neural network for prediction method of path loss characteristics considering diffraction and reflection in an open-square environment," in *Proc. URSI Asia–Pacific Radio Sci. Conf. (AP-RASC)*, Mar. 2019, pp. 1–3.

[30] L. Wu, D. He, B. Ai, J. Wang, H. Qi, K. Guan, and Z. Zhong, "Artificial neural network based path loss prediction for wireless communication network," *IEEE Access*, vol. 8, pp. 199523–199538, 2020.

[31] H. F. Ates, S. M. Hashir, T. Baykas, and B. K. Gunturk, "Path loss exponent and shadowing factor prediction from satellite images using deep learning," *IEEE Access*, vol. 7, pp. 101366–101375, 2019.

[32] S. Y. Seidel and T. S. Rappaport, "A ray tracing technique to predict path loss and delay spread inside buildings," in *Proc. IEEE Global Telecommun. Conf.*, vol. 2, Dec. 1992, pp. 649–653.

[33] M. Charitos, D. Kong, J. Cao, D. Berkovskyy, A. A. Goulianos, T. Mizutani, F. Tila, G. Hilton, A. Doufexi, and A. Nix, "LTE-A virtual drive testing for vehicular environments," in *Proc. IEEE 85th Veh. Technol. Conf. (VTC Spring)*, Jun. 2017, pp. 1–5.

[34] J. Thrane, D. Zibar, and H. L. Christiansen, "Model-aided deep learning method for path loss prediction in mobile communication systems at 2.6 GHz," *IEEE Access*, vol. 8, pp. 7925–7936, 2020.

[35] S. Y. Han, N. B. Abu-Ghazaleh, and D. Lee, "Efficient and consistent path loss model for mobile network simulation," *IEEE/ACM Trans. Netw.*, vol. 24, no. 3, pp. 1774–1786, Jun. 2016.

[36] G. R. Maccartney, T. S. Rappaport, S. Sun, and S. Deng, "Indoor office wideband millimeter-wave propagation measurements and channel models at 28 and 73 GHz for ultra-dense 5G wireless networks," *IEEE Access*, vol. 3, pp. 2388–2424, 2015.

[37] S. Sun, T. S. Rappaport, T. A. Thomas, A. Ghosh, and H. C. Nguyen, "Investigation of prediction accuracy, sensitivity, and parameter stability of large-scale propagation path loss models for 5G wireless communications," *IEEE Trans. Veh. Technol.*, vol. 65, no. 5, pp. 2843–2860, May 2016.

[38] T. S. Rappaport, G. R. Maccartney, M. K. Samimi, and S. Sun, "Wideband millimeter-wave propagation measurements and channel models for future wireless communication system design," *IEEE Trans. Commun.*, vol. 63, no. 9, pp. 3029–3056, Sep. 2015.

[39] A. Bhuvaneshwari, R. Hemalatha, and T. Satyasavithri, "Semi deterministic hybrid model for path loss prediction improvement," *Proc. Comput. Sci.*, vol. 92, pp. 336–344, Dec. 2016.

[40] A. M. Al-samman, T. Abd Rahman, and M. H. Azmi, "Indoor corridor wideband radio propagation measurements and channel models for 5G millimeter wave wireless communications at 19 GHz, 28 GHz, and 38 GHz bands," *Wireless Commun. Mobile Comput.*, vol. 2018, Mar. 2018, Art. no. 6369517.

[41] G. R. MacCartney, J. Zhang, S. Nie, and T. S. Rappaport, "Path loss models for 5G millimeter wave propagation channels in urban microcells," in *Proc. IEEE Global Commun. Conf. (GLOBECOM)*, Dec. 2013, pp. 3948–3953.

[42] E. I. Adegoke, E. Kampert, and M. D. Higgins, "Empirical indoor path loss models at 3.5GHz for 5G communications network planning," in *Proc. Int. Conf. UK-China Emerg. Technol. (UCET)*, Aug. 2020, pp. 1–4.

[43] E. I. Adegoke, E. Kampert, and M. D. Higgins, "Channel modeling and Over-the-Air signal quality at 3.5 GHz for 5G new radio," *IEEE Access*, vol. 9, pp. 11183–11193, 2021.

[44] A. Al-Samman, T. Rahman, M. Hindia, A. Daho, and E. Hanafi, "Path loss model for outdoor parking environments at 28 GHz and 38 GHz for 5G wireless networks," *Symmetry*, vol. 10, no. 12, p. 672, Nov. 2018.

[45] A. M. Al-Samman, T. A. Rahman, M. H. Azmi, A. Sharaf, Y. Yamada, and A. Alhammadi, "Path loss model in indoor environment at 40 GHz for 5G wireless network," in *Proc. IEEE 14th Int. Colloq. Signal Process. Appl. (CSPA)*, Mar. 2018, pp. 7–12.

[46] S. Li, Y. Liu, L. Lin, D. Sun, S. Yang, and X. Sun, "Simulation and modeling of millimeter-wave channel at 60 GHz in indoor environment for 5G wireless communication system," in *Proc. IEEE Int. Conf. Comput. Electromagn. (ICCEM)*, Mar. 2018, pp. 1–3.

[47] G. R. Maccartney, T. S. Rappaport, M. K. Samimi, and S. Sun, "Millimeter-wave omnidirectional path loss data for small cell 5G channel modeling," *IEEE Access*, vol. 3, pp. 1573–1580, 2015.

[48] A. M. Al-Samman, M. H. Azmi, Y. A. Al-Gumaei, T. Al-Hadhrami, T. A. Rahman, Y. Fazea, and A. Al-Mqdashi, "Millimeter wave propagation measurements and characteristics for 5G system," *Appl. Sci.*, vol. 10, no. 1, p. 335, Jan. 2020.

[49] A. M. Al-Samman, T. Abd. Rahman, T. Al-Hadhrami, A. Daho, M. N. Hindia, M. H. Azmi, K. Dimyati, and M. Alazab, "Comparative study of indoor propagation model below and above 6 GHz for 5G wireless networks," *Electronics*, vol. 8, no. 1, p. 44, Jan. 2019.

[50] I. Cuinas, M. G. Sanchez, A. Feys, W. Debaenst, and J. Verhaevert, "Indoor path loss variations with frequency and visibility conditions at 3.5 GHz band," in *Proc. IEEE Int. Symp. Antennas Propag. USNC-URSI Radio Sci. Meeting*, Jul. 2019, pp. 2069–2070.

[51] N. Khalid, N. A. Abbasi, and O. B. Akan, "Statistical characterization and analysis of low-THz communication channel for 5G Internet of Things," *Nano Commun. Netw.*, vol. 22, Dec. 2019, Art. no. 100258.

[52] F. Qamar, M. N. Hindia, K. Dimyati, K. A. Noordin, M. B. Majed, T. A. Rahman, and I. S. Amiri, "Investigation of future 5G-IoT millimeter-wave network performance at 38 GHz for urban microcell outdoor environment," *Electronics*, vol. 8, no. 5, p. 495, May 2019.

[53] Y. Zhou, X. Sun, P. Zhang, H. Wang, Z. Hu, and H. Wang, "Multi-frequency millimeter-wave large-scale path loss characterization for indoor environment," in *Proc. Int. Symp. Antennas Propag. (ISAP)*, Feb. 2019, pp. 1–3.

[54] J. Wen, Y. Zhang, G. Yang, Z. He, and W. Zhang, "Path loss prediction based on machine learning methods for aircraft cabin environments," *IEEE Access*, vol. 7, pp. 159251–159261, 2019.

[55] H. Cheng, S. Ma, H. Lee, and M. Cho, "Millimeter wave path loss modeling for 5G communications using deep learning with dilated convolution and attention," *IEEE Access*, vol. 9, pp. 62867–62879, 2021.

[56] N. Kuno and Y. Takatori, "Prediction method by deep-learning for path loss characteristics in an open-square environment," in *Proc. Int. Symp. Antennas Propag. (ISAP)*, 2018, pp. 1–2.

[57] A.-Y. Hsiao, C.-F. Yang, T.-S. Wang, I. Lin, and W.-J. Liao, "Ray tracing simulations for millimeter wave propagation in 5G wireless communications," in *Proc. IEEE Int. Symp. Antennas Propag. USNC/URSI Nat. Radio Sci. Meeting*, Jul. 2017, pp. 1901–1902.

[58] C. Ge, Y. Zhang, and X. Jiang, "Simulation and analysis of 28 GHz millimeter-wave propagation characteristics in typical residential house environment," in *Proc. 11th UK-Eur.-China Workshop Millim. Waves THz Technol. (UCMMT)*, 2018, vol. 1, pp. 1–3.

[59] K. Kitao, A. Benjebbour, T. Imai, Y. Kishiyama, M. Inomata, and Y. Okumura, "5G System Evaluation Tool," in *Proc. IEEE Int. Workshop ElectroMagn., Appl. Student Innov. Competition*, Dec. 2018, pp. 1–2.

[60] F. Hossain, T. Geok, T. Rahman, M. Hindia, K. Dimyati, S. Ahmed, C. Tso, and N. A. Rahman, "An efficient 3-D ray tracing method: Prediction of indoor radio propagation at 28 GHz in 5G network," *Electronics*, vol. 8, no. 3, p. 286, Mar. 2019.

[61] C.-F. Yang, B.-C. Wu, and C.-J. Ko, "A ray-tracing method for modeling indoor wave propagation and penetration," *IEEE Trans. Antennas Propag.*, vol. 46, no. 6, pp. 907–919, Jun. 1998.
[62] A. E. Shaikh, F. Majeed, M. Zeeshan, T. Rabbani, and I. Sheikh, "Efficient implementation of deterministic 3-D ray tracing model to predict propagation losses in indoor environments," in *Proc. 13th IEEE Int. Symp. Pers., Indoor Mobile Radio Commun.*, Oct. 2002, pp. 1208–1212.
[63] V. V. Diaz and D. Marcano Aviles, "A path loss simulator for the 3GPP 5G channel models," in *Proc. Int. Conf. Electron., Electr. Eng. Comput. (INTERCON)*, Aug. 2018, pp. 1–4.
[64] U. R. Kamboh, U. Ullah, S. Khalid, U. Raza, C. Chakraborty, and F. Al-Turjman, "Path loss modelling at 60 GHz mmWave based on cognitive 3D ray tracing algorithm in 5G," *Peer Netw. Appl.*, vol. 14, no. 5, pp. 3181–3197, Sep. 2021.
[65] E. G. Observatory. (2018). *Major International 5G trials and Pilot*. [Online]. Available: https://5gobservatory.eu/5g-trial/major-international-5g-trials-and-pilots/
[66] T. S. Rappaport, S. Sun, R. Mayzus, H. Zhao, and Y. Azar, "Millimeter wave mobile communications for 5G cellular: It will work!" *IEEE Access*, vol. 1, pp. 335–349, 2013.
[67] G. S. Karthikeya, M. P. Abegaonkar, and S. K. Koul, "Path loss compensated co-polarized stacked antennas with progressive offset ZIM for mmWave 5G base stations," in *Proc. Int. Conf. Electromagn. Adv. Appl. (ICEAA)*, Sep. 2019, pp. 0355–0356.
[68] H. Wang, P. Zhang, J. Li, and X. You, "Radio propagation and wireless coverage of LSAA-based 5G millimeter-wave mobile communication systems," *China Commun.*, vol. 16, no. 5, pp. 1–18, May 2019.
[69] T. S. Rappaport, *Wireless Communications: Principles and Practice*. Upper Saddle River, NJ, USA: Prentice-Hall, 2002.
[70] S. I. Popoola, A. Jefia, A. A. Atayero, O. Kingsley, and N. Faruk, "Determination of neural network parameters for path loss prediction in very high frequency wireless channel," *IEEE Access*, vol. 7, pp. 150462–150483, 2019.

SIMON K. HINGA (Graduate Student Member, IEEE) received the B.Sc. degree in electrical and electronic engineering from the Technical University of Mombasa, Kenya, in 2016, and the Postgraduate Diploma degree in satellite communication engineering from African Regional Center for Space Science and Technology Education-English (Affiliated to United Nations), in 2018. He is currently pursuing the M.Eng. degree in information and communication engineering with Covenant University, Nigeria. He is sponsored by Queen Elizabeth Commonwealth Scholarship. His research interests include mmWave, satellite communications, the Internet of Things, emerging technology, and machine learning application in wireless communications. He is a member of IEEE Communication Society (ComSoc), IEEE Antenna and Propagation Society, and IEEE Sensors Council.

ADEREMI A. ATAYERO (Member, IEEE) is a passionate educationist at the vanguard of the transformation in African Higher Education. He is also recognised for contemporary multidisciplinary academic research with special focus on wireless/mobile communications, the Internet of Things (loT), and smart cities. He has a progressive academia leadership experience on developing team members and collaborating regionally and globally to maintain the competitive edge in world-class education. His research interests include communication engineering, including wireless sensor networks, wireless (mobile) communications, the Internet of Things (IoT), and smart cities.